Project porcupine : the MF mutual-impedance probe experiment. Part I : Flight F2 (March 1977)

L.R.O. Storey, J. Thiel, J.M. Illiano

CENTRE NATIONAL D'ETUDES DES TELECOMMUNICATIONS

CENTRE NATIONAL DE LA RECHERCHE SCIENTIFIQUE

CENTRE DE RECHERCHES EN PHYSIQUE DE L'ENVIRONNEMENT TERRESTRE ET PLANETAIRE

CRPE

NOTE TECHNIQUE
C.R.P.E. 93

PROJECT PROCUPINE

THE MF MUTUAL :- IMPEDANCE PROBE EXPERIMENT PART 1 :- FLIGHT F 2 (MARCH 1977)

by

L.R.O. STOREY . J. THIEL and J.M. ILLIANO

C.R.P.E. / R.P.E.
45045 ORLEANS CEDEX.

CENTRE NATIONAL D'ETUDES
DES TELECOMMUNICATIONS

CENTRE NATIONAL DE
LA RECHERCHE SCIENTIFIQUE

CENTRE DE RECHERCHES EN PHYSIQUE DE
L'ENVIRONNEMENT TERRESTRE ET PLANETAIRE

NOTE TECHNIQUE CRPE/93

PROJECT PORCUPINE

THE MF MUTUAL-IMPEDANCE PROBE EXPERIMENT

PART 1 : - FLIGHT F2 (MARCH 1977)

by

L.R.O. STOREY, J. THIEL, and J.M. ILLIANO

C.R.P.E./R.P.E.

45045 ORLEANS CEDEX

le 1er Mars 1981

ABSTRACT

Results are presented from a medium-frequency (0.1 - 1.5 MHz) mutual-impedance probe flown on the three rockets in the auroral ionosphere. The main purpose of these experiments was to measure the field-aligned drift velocity of the thermal electrons, from the resulting non-reciprocal frequency-shift of the lower oblique resonance. In the first experiment (Porcupine F2), the data exhibited frequency-shifts much larger than expected, and which varied cyclically as the payload spun. These spurious shifts, which were partly of technological origin, masked any shifts due to field-aligned drift. They led to a redesign of the probe. In the second experiment (Porcupine F3), the data were consistent with downward electron drifts, but their apparent high velocity casts doubt on this interpretation. The data from the third experiment (Porcupine F4) exhibited frequency-shifts that clearly were related to the cross-field drift of the plasma under the influence of the perpendicular component of the auroral electric field, but again they were larger than the values expected theoretically. The conclusions are that this method for measuring field-aligned electron drift velocity is not yet ready for scientific use, but that it would become useful if its sensitivity could be improved by an order of magnitude. Suggestions are made as to how this improvement might be achieved.

CONTENTS

PART 1 - FLIGHT F2 (MARCH 1977)

PREFACE

The experiment described in this report was a contribution from the Centre for Research in Environmental Physics (CRPE) of the French National Centre for Scientific Research to the West-German "Porcupine" program of rocket research on auroral physics during the International Magnetospheric Study.

The report is divided into two parts, the first being concerned with a rocket flight in March 1977, and the second with the two remaining flights in March 1979.

Part 1 of the report is arranged as follows. In Section 1, the Porcupine MF probe experiment is outlined in the context of current auroral research. In Section 2, the principles of the measurement of electron drift velocity by means of an MF mutual-impedance probe are explained briefly . Section 3 contains a technical description of the rocket-borne instruments, in their original form as used on the March 1977 flight. Section 4 describes the results from this flight : the technical performance of the instruments, the scientific results obtained, and their possible interpretations are presented in turn. Finally, in Section 5 there is a discussion of the provisional conclusions that were drawn from these results, and formed the basis for the modifications that were made to the instruments in preparation for the flights in March 1979. These last two flights are the subject of Part 2 of the report*.

*Note. The references cited in Part 1 are listed at the end of Part 2, together with those cited in Part 2.

1. INTRODUCTION

1.1. THE PORCUPINE PROGRAM

The Porcupine program involved three Aries rockets which were launched from the ESRANGE at Kiruna, Sweden (Geographic coordinates : 67° 53' N, 21° 04' E) on 20 March 1977, and on 19 and 31 March 1979. We shall refer to these three flights as F2, F3 and F4 respectively ; an initial flight F1, in March 1976, was unsuccessful due to failure of the rocket motor.

Each of the three scientific payloads contained a variety of experiments for studying the energetic particles and the plasma, together with the quasi-static and wave fields, both electric and magnetic. A list of these experiments is given in Table 1. They included four ejectable sub-payloads, as follows : two barium ion-jet canisters, of which one functioned correctly on F2 ; a cesium plasma source, which failed to function on F2, and was replaced by a xenon plasma source on F3 and F4 ; a free-flying probe equipped for a number of experiments, as listed in Table 2. The composition of the payload, and also the design of some of the experiments, were modified slightly between the 1977 flight F2, and the flights F3 and F4 in 1979. A summary of the scientific objectives and instrumentation for Project Porcupine has been edited by *Haerendel* [1976], while detailed technical information on the payloads has been given by *Joneleit* [1976], by *Schmitt* [1979] and by *Häusler* [1981] ; the last two of these documents contain the launch data for the three flights.

One of the main aims of the Porcupine program was to gain a better understanding of the acceleration mechanisms for auroral particles, and the emphasis of the investigation was on the currently most favoured mechanism involving quasi-static electric fields parallel to the earth's magnetic field. Such fields have been observed directly in the altitude range 1,000 - 10,000 km [*Haerendel et al.*, 1976 ; *Westcott et al.*, 1977 ; *Mozer et al.*, 1977, 1980 ; *Mozer*, 1980]. Though there is some evidence that they may exist at lower altitudes, even below 500 km [*Sojka et al.*, 1976 ; *Mozer*, 1980], this is generally regarded as controversial. At F-region altitudes, to which the present experiments were restricted, the fields responsible for auroral particle acceleration are observable only in various indirect ways : by observing the local electric fields - mainly perpendicular to the magnetic

field - which form part of the same large-scale system ; by observing the accelerated particles, together with the secondaries that they produce through their interaction with the atmosphere ; by observing the electromagnetic waves that are generated somehow as a by-product of the acceleration process ; finally, by observing the associated electric currents, which flow mainly horizontally in the E-region but are field-aligned in the F region and above. The principal objective of the experiment here described had to do with measuring these field-aligned currents.

1.2. FIELD-ALIGNED CURRENTS

Up to now, such currents have been observed mainly through their magnetic effects [*Cloutier and Anderson*, 1975 ; *Russell*, 1977]. These are related to the density of the total current, irrespective of which particles are carrying it. Unfortunately the relationship is not a local one : for static fields, the current density is equal to the curl of the magnetic field perturbation. Hence the relevant magnetic data, from 3-axis magnetometers on rockets or on polar-orbiting satellites, are usually analysed on the assumption that the distribution of current is uniform in the magnetic east-west direction, i.e. that the currents flow in sheets extended along parallels of magnetic latitude [*Zmuda and Armstrong*, 1974]. Perturbations due to any other type of structure are misinterpreted. Clearly there is a need for some means of making local measurements of field-aligned current density.

The contribution made to the field-aligned current by any one type of energetic charged particle can be determined locally by measuring its distribution function, in energy and in pitch angle, with a suitable analyser, and then integrating this distribution so as to obtain the total parallel flux [*Anderson and Vondrak*, 1975]. In the ionosphere, this method works satisfactorily for the positive ions, but they carry only a small fraction of the current. For the electrons, it can be used at energies above about 5 eV : at lower energies, perturbations of the particle trajectories near to the analyser make the measurement extremely difficult. At present, there is no reliable method for determining the parallel flux of thermal electrons, which is regrettable because upgoing thermal electrons appear to be the main carriers of downward field-aligned currents [*Cloutier et al.*, 1970 ; *Arnoldy*, 1974 ; *Theile and Wilhelm*, 1980].

The relevance of downward currents to auroral particle acceleration is that, at high altitudes, they may drive instabilities, and so produce plasma turbulence, enhanced resistivity, and downward-directed parellel electric fields [*Kindel and Kennel*, 1971]. Such fields would accelerate auroral protons downwards, and also electrons upwards. Upward field-aligned fluxes of low-energy (< 1 keV) suprathermal electrons have been observed as low as 1400 km [*Klumpar et al.*, 1976], but the evidence for downward field-aligned fluxes of energetic protons at lower altitudes is meagre [*Hultqvist et al.*, 1971 ; *Reme and Bosqued*, 1971] ; nevertheless such fluxes have been observed in all local-time sectors, and in periods of weak as well as of strong magnetic activity [*Sauvaud*, 1977]. These inconclusive results contrast with the overwhelming evidence for downward acceleration of auroral electrons by upward-directed parallel electric fields during periods of strong activity [*Evans*, 1975]. It is uncertain what proportion of the associated upward field-aligned currents are carried, in the F region, by thermal electrons, and it would be interesting to know this.

1.3. METHOD OF MEASUREMENT

Let us return, therefore, to the question of how to measure the thermal-electron component of field-aligned currents. A method for direct local measurement of the field-aligned drift velocities of the thermal electrons has been proposed by *Storey and Pottelette* [1971]. It is based on the artificial excitation and propagation of electrostatic waves in the ionospheric plasma, under linear conditions, at frequencies sufficiently high that the waves are supported entirely by the electrons ; since the thermal electrons are in a large majority, they govern the properties of the waves. In the proposed experiment, electron plasma waves are propagated between two antennas separated by a distance of a few tens of electron Larmor radii. If the thermal electrons as a whole are stationary with respect to the antenna system, then the electrical characteristics of this radio link are independent of the direction of transmission, i.e.they remain the same if the roles of emission and reception are exchanged between the two antennas. On the other hand, if the thermal electrons are drifting in a direction such that they bulk velocity has a component along the line joining the two antennas, then their drift motion destroys the symmetry of the link ; in engineering parlance, the system becomes *non-reciprocal*. For a given wave frequency and given plasma parameters, the difference between the characteristics of the link for the two directions of propagation can be used to determine the drift

velocity, so long as its direction is known apart from the sign (for instance, if the velocity is known to be field-aligned, but may be directed either upwards or downwards). The velocity thus determined, multiplied by their number density, yields the flux of thermal electrons along the field, and hence their contribution to the field-aligned current.

The proposal of *Storey and Pottelette* [1971] involved the linear transmission of electrostatic waves at frequencies near that of the lower oblique resonance (LOR) of the plasma, where the nonreciprocal effects of field-aligned electron drift are particularly marked. The LOR frequency lies in a range bounded at the bottom by the lower hybrid resonance frequency, and at the top by the plasma frequency or the electron gyrofrequency, whichever is the smaller. Its exact value depends not only on the plasma parameters, but also on the angle that the transmission path between the two antennas makes with the magnetic field ; for detecting the effects of field-aligned drift, angles of 30° - 60° are quite suitable. Then, in the auroral F region, the LOR frequency is typically in the range 0.5 - 1.0 MHz. We call these *medium frequencies* (MF), and the system of two antennas and associated electronics is the *MF probe*.

The most useful effect for present purposes is a shift in the LOR frequency at a given angle. The magnitude of the frequency-shift is an increasing function of the drift velocity, linear at small values, while the sign is that of the component of the velocity in the direction going from the emitting antenna to the receiving antenna, so it changes when the direction of transmission is reversed. This effect, which was predicted theoretically [*Storey and Pottelette*, 1971], has been observed in a laboratory plasma by *Illiano and Pottelette* [1979]. The theory has been developed by *Pottelette* [1973, 1977] for a cold magnetoplasma, by *Kuehl* [1974] for a warm magnetoplasma but in the limit of very small velocities, and by *Singh* [1977] for a warm magnetoplasma but with an infinite magnetic field. Subsequently *Singh* [1980] extended his work to the case where the electron distribution function is non-Maxwellian. *Storey and Thiel* [1978] assumed a displaced Maxwellian distribution, but avoided all restrictions on the electron temperature, magnetic field strength, and drift velocity ; this study was performed in support of the Porcupine experiments.

Of course, these are by no means the first experiments in which the LOR has been excited artificially and observed in the ionosphere. Limiting the review to experiments in which the resonance was excited by some kind of antenna, the first was that of *Koons et al.* [1974] on a polar-orbiting satellite in the altitude range 1500-2000 km. Subsequently *Gonfalone* [1974] and *Michel et al.* [1975] performed similar experiments on rockets in the ionosphere. The antennas used by Koons et al. were small dipoles, while the other experimenters used small monopoles. In all cases, the emitting antenna was excited at a fixed frequency, and the resonance was observed as a maximum in the variation of the electric field or potential as a function of the angle between the transmission path and the earth's magnetic field ; this angle varied cyclically because of the spin of the vehicle. This is not the best way to observe the effects of drift, and indeed none were detected.

The present experiment was the first in which arrangements were made deliberately in order to detect such effects. First and foremost, rather than hold the transmitted frequency constant and let the angle between the transmission path and the magnetic field vary, this angle was held as constant as possible while the frequency was swept repeatedly through a range spanning the LOR. Under these circumstances, as already noted, any field-aligned drift of the thermal electrons should shift the LOR frequency upward or downward depending on the direction of transmission. This direction was reversed repeatedly, so that two response curves, one for each direction, were traced out in the course of each frequency-sweep. The drift should have revealed itself by shifting the maximum of one of the curves with respect to the other.

1.4. ORDERS OF MAGNITUDE

Near the peak of the F region, the expected frequency-shifts are rather small. In general, the relative shift (i.e. the shift expressed as a fraction of the mean resonance frequency for the two directions of transmission) is of the same order of magnitude as the ratio of the parallel drift velocity to the electron thermal velocity. Now, if the contribution of the ions is neglected, the parallel current density $j_{//}$ is proportional to the product of the drift velocity $V_{//}$ and of the electron density N :

(1) $$j_{//} = N e V_{//}$$

e is the electronic charge. The highest current densities that have been inferred from observations by rocket-borne magnetometers are of the order of 10^{-4} A/m^2 [*Anderson and Vondrak*, 1975]. If, for the electron density, we take 10^{11} m^{-3} as a typical value, then the corresponding drift velocity is approximately 6 km/s. Taking the electron thermal velocity as $V_{th} = (2 k T_e/m_e)^{1/2}$ where k is Boltzmann's constant and m_e the electron mass, its value is 213 km/s for a typical electron temperature T_e of 1500 K. Hence the relative frequency-shift is no more than about 3 %, which is likely to be only just detectable.

Clearly the chances of detecting the LOR frequency-shift near the F-region peak, and of being able to use it to measure the field-aligned drift velocity $V_{//}$ of the thermal electrons, would be enhanced if the rocket were to encounter currents of greater density than the magnetometer observations, with their limited spatial resolution, have led us to expect. That such intense field-aligned currents do indeed exist is suggested by the discovery of the electrostatic ion cyclotron instability in the F region, around 370 km altitude [*Bering et al.*, 1975], and also in the upper E region [*Martelli et al.*, 1977] ; moreover, *D'Angelo* [1973] has argued that type III spectra of the radio aurora can be interpreted in terms of unstable electrostatic ion cyclotron waves. If the electron and ion temperatures are of the same order, this instability cannot be excited in the F region, where the ions are mainly O^+ and collisions are negligible, unless the drift velocity exceeds about 10 % of the electron thermal velocity [*Kindel and Kennel*, 1971]. In the upper E region, the ions are heavier and the electron temperature is lower, both of which factors tend to lower the threshold of instability, but on the other hand ion-neutral collisions are more frequent, which has the opposite effect, so probably the threshold is much the same as it is in the F region. Parallel drift velocities of this magnitude would certainly give rise to detectable LOR frequency-shifts.

Therefore it is interesting to note that quite common field-aligned current densities, such as 10^{-5} A/m^2, correspond to drift velocities of this magnitude in the relatively tenuous plasma of the topside F region. Since the current is conserved in any tube of magnetic flux, and since the cross-

sectional area of a flux tube varies with altitude only on the scale of the radius of the earth, the current density is almost constant along a field line at altitudes much less than an earth radius. Hence the value of $V_{//}$ increases, in accordance with (1), as N decreases with increasing altitude. It follows that the predicted frequency-shifts would certainly be observable if the experiment were performed well above the F-region peak, for instance at altitudes in the range 750-1500 km.

A further obstacle to the detection, at F-region altitudes, of the LOR frequency-shifts due to field-aligned currents, is the existence of perpendicular (i.e. cross-field) plasma drifts, due to the perpendicular component of the ionospheric electric field. These drifts also can attain velocities of several km/s, and they should give rise to frequency-shifts of the same order of magnitude as those due to field-aligned drift. In theory, however, the effects of perpendicular drift can be allowed for if its velocity is known, for instance from independent measurements of the ambient electric field. Moreover, although the perpendicular drift velocity increases with altitude, in accordance with the geometry of the earth's magnetic field, it does so much less rapidly than the parallel drift velocity does. This is another reason why the frequency-shifts due to field-aligned currents should be more conspicuous at greater altitudes, and why the Porcupine experiments, performed in the auroral F region, were a particularly stringent test of the ability of the MF mutual-impedance probe to detect and to measure them.

2. PRINCIPLES

2.1. EFFECTS OF ELECTRON DRIFT

In trying to explain the principles of the present method for measuring the electron drift velocity, a convenient starting-point is the quasi-electrostatic potential created in a magnetoplasma by an alternating point charge $q = q_o \exp(i\omega t)$. We take the source to be at the origin of coordinates, and consider the spatial distribution of potential in its vicinity.

If the plasma is cold and collisionless, then in certain ranges of the excitation frequency $f = \omega/2\pi$ this potential is infinite in all directions that make either a certain angle β_c or its complement $\pi - \beta_c$ with the magnetic field ; the value of β_c depends on the frequency. Such an oblique resonance, the LOR, exists in part of the frequency range in which electromagnetic waves are propagated in the whistler mode, namely the part above the lower-hybrid frequency. The angles β_c and $\pi - \beta_c$ correspond to the ray directions in which the group velocity of the waves is zero, so their energy accumulates. The two sets of all such directions form the two *resonance cones*, with their apexes joined at the source and pointing in opposite directions with respect to the magnetic field.

If the thermal motion of the electrons is taken into account, then the resonance is found to be damped. Instead of becoming infinite, the variation of the potential with direction at a fixed distance from the source attains a finite maximum at some angle β_o slightly different from β_c, and smaller secondary maxima appear [*Fisher and Gould*, 1971 ; *Singh and Gould*, 1971, 1973]. The resonance-cone angle β_o may be greater or less than β_c, and the subsidiary maxima may be inside or outside the resonance cone, depending on the frequency and on the distance [*Storey et al.*, 1980]. Fig. 1a gives an example of the directional variation of the potential in a warm plasma, as calculated from the theory of *Storey and Thiel* [1978]. This figure is a polar graph of $|\psi|$, where ψ is the potential normalized with respect to its vacuum value. The calculations were made for the case where the plasma frequency is five times the electron gyrofrequency, and the excitation frequency is half the gyrofrequency ; the distance between the point source and the point of observation is 90 electron Larmor radii.

The resonance-cone angle β_o depends on the frequency of excitation : for the LOR, it always increases with increasing frequency. This fact is illustrated in Figure 2a, where, in each of the three panels, the point in the middle represents the source, the magnetic field vector is vertical, and the broken line is in a direction making a fixed angle β with the field. The panel on the left represents an initial situation, at a frequency such that this direction lies on the resonance cone ($\beta_o = \beta$). Then, if the frequency is decreased (central panel) the cone contracts ($\beta_o < \beta$), degenerating into a line parallel to $\mathbf{B_o}$ at the lower hybrid frequency, while if the frequency is increased (right-hand panel) the cone expands ($\beta_o > \beta$), and degenerates into a disc perpendicular to $\mathbf{B_o}$ at the upper frequency limit for the LOR, which was specified in § 1.3.

As the frequency of excitation increases and the resonance cone expands, the amplitude of the potential at the resonance decreases, when all other things are equal.

If, in addition to their random thermal velocities, the electrons have a systematic drift velocity $\mathbf{V}$ along the magnetic field, then the directional variation of the potential is modified (see Figure 1b, in which we have taken $V = 0.16\ V_{th}$). The resonance cones react as if they were flexible and were being dragged downstream. The upper cone in the figure, which opens in the direction parallel to $\mathbf{B_o}$, now becomes narrower ; here, downstream, the resonance-cone angle β_{+o} is less than the value β_o in the absence of drift. The lower cone, which opens against the oncoming electron stream, becomes wider ($\beta_{-o} < \pi - \beta_o$). The subscripts + and - refer to the sign of the scalar product $\mathbf{V}.\mathbf{B_o}$. Since we have assumed that $\mathbf{V}$ is parallel to $\mathbf{B_o}$, and since we have defined β as the angle between $\mathbf{B_o}$ and the radius vector $\mathbf{r}$ from the source to the point of observation, both the contraction of the downstream cone and the expansion of the upstream cone correspond to decreases of the resonance-cone angles : had we taken $\mathbf{V}$ as being anti-parallel to $\mathbf{B_o}$, then both of the resonance-cone angles would have increased, but this is simply a result of the convention adopted in the definition of β. The left-hand panel of Figure 2b illustrates this behaviour, in a situation similar to that of the corresponding panel in Figure 2a, but where the electrons have been given a field-aligned velocity upwards, parallel to $\mathbf{B_o}$. These theoretical predictions have been confirmed by experiments in laboratory plasmas [*Lucks and Kramer*, 1980 ; *Boswell and Thiel*, 1981].

The theory also predicts that the maximum amplitude of the potential should be raised on the upstream cone and lowered on the downstream cone. In the case illustrated in Figure 11b, the difference in the two amplitudes in only about 5 %, so it is not very noticeable. Apparently no effort has been made to confirm this prediction.

In the present experiments, our method for detecting field-aligned electron drift velocity was to measure, not the directional variation of the potential at fixed frequency, but its frequency variation in two fixed and opposite directions inclined to the magnetic field. In the absence of drift, at a fixed distance from the source and in a fixed direction characterized by the angle β, the variation of the potential ψ as a function of the frequency f is the same as it is in the opposite direction, at the angle $\pi - \beta$. For our purposes, the choice of β was not critical, and we took $\beta \simeq 30°$. With β fixed, let $f_o(\beta)$ be the frequency at which $|\psi(f)|$ is maximum. This resonance frequency is almost the same as the frequency at which the resonance-cone angle β_o is equal to β, though it is not exactly the same because $|\psi(\beta_o)|$ varies with frequency. Now, in a stationary plasma $f_o(\beta) = f_o(\pi - \beta)$, but this is no longer true in the presence of field-aligned drift, which robs the potential distribution $\psi(\mathbf{r})$ of its reflection symmetry about the plane perpendicular to $\mathbf{B_o}$ passing through the source, while leaving intact the azimuthal symmetry about the magnetic field line through the source. In the upstream direction, where the effect of the drift is to widen the resonance cone, the frequency of excitation must be reduced if the resonance cone is to be brought back into the direction of observation. Thus, for observations upstream in the direction $\pi - \beta$, the frequency f_{-o} of maximum $|\psi(f)|$ is less than f_o (central panel). Conversely, for observations downstream in the direction β, the resonance frequency is raised : $f_{+o} > f_o$ (right-hand panel). As a further result of the drift, the maximum value of $|\psi(f)|$ is increased in the upstream and reduced in the downstream direction. These various effects are exhibited in Figure 1c, which has been reproduced from Figure 9 of the paper by *Storey and Thiel* [1978] ; ψ_- is the potential upstream, and ψ_+ the potential downstream.

In Figure 1c, it is noticeable that the difference in the maximum amplitudes of the potential upstream and downstream, which amounts to about 7.5 %, is greater than it is in Figure 1b. This is due to the difference in the frequencies of the upstream and downstream resonances.

Evidently, according to the theory, the magnitude and sign of the field-aligned drift velocity can be determined by measuring the difference in the frequencies and/or amplitudes of the LOR observed in the two opposite directions ; for Porcupine, we concentrated on the frequency-shifts in the belief that they could be measured more accurately than the changes in amplitude.

The effects of cross-field plasma drift on $|\psi(f)|$ measured in two opposite directions can be understood by reasoning similar to the above. Again, the drift motion drags the resonance cones downstream ; see Figure 2c, in which the stream of electrons is coplanar with $\mathbf{B}_o$ and the directions of observation, and it is coming from the right. The drift now destroys the azimuthal symmetry of the potential, while preserving the reflection symmetry. Contrary to the previous case, the resonance frequency f_o is lowered in the downstream direction (central panel) and raised in the upstream direction (right-hand panel). No quantitative theoretical study of these effects has yet been made, nor have they been observed experimentally in the laboratory.

The qualitatively similar effects of field-aligned and of cross-field drift are distinguishable because the latter depend on the azimuth of the direction of observation around the axis formed by the magnetic field line passing through the source. If the azimuth is changed by π radians (180°), then the resonance frequency that was observed previously at the angle β to the field is now observed at $\pi - \beta$, and vice versa. Thus if measurements are made of the difference Δf between the resonance frequencies observed in opposite directions, and if these two directions are rotated about the field-line through the source, then Δf does not vary when it is due to field-aligned drift. On the other hand, when it is due to cross-field drift, Δf takes its largest positive or negative values at the azimuths where these directions lie in the plane defined by the magnetic field and the drift-velocity vector ; half-way between these two azimuths, the directions of observation are perpendicular to the cross-field drift velocity and Δf vanishes. In the general case, where the drift velocity vector has field-aligned and cross-field components simultaneously, both components should be derivable from measurements of Δf as a function of azimuth.

2.2. DESIGN OF THE SENSOR

We must now consider some slightly more practical questions about the design of an antenna system, or *sensor*, for making the measurements discussed above, namely what sort of electrodes should be used, how many are required, and how they should be disposed. The foregoing theoretical discussion was concerned with the potential that an alternating point charge creates at a neighbouring point in the plasma. In practice, both for emitting charge into the plasma and for measuring the resultant potential, it is necessary to use electrodes of finite size ; generally these are spheres, with radii much smaller than the distance between them, so as to approximate point contacts with the plasma. Moreover, two electrodes are not enough : since charge is conserved, another electrode is needed at the emitting end of the system, in order to close the circuit through the plasma ; equally, at the receiving end, another electrode is required to provide a point of reference for the measurement of the potential. These considerations suggest two basic arrangements for the electrodes, which we call *double-monopole* and *double-dipole* (or *quadripole*) layouts [*Storey et al.*, 1969]. In double-monopole layouts, the additional electrodes mentioned above are one and the same, and are formed either by the conducting wall of the plasma chamber in laboratory experiments [*Illiano and Pottelette*, 1979 ; *Lucks and Kramer*, 1980 ; *Boswell and Thiel*, 1981], or by the conducting body of the vehicle in space experiments [*Gonfalone*, 1974 ; *Michel et al.*, 1975]. This arrangement has the advantage of simplicity, but also the disadvantage that the self-impedance of the large third electrode is common to the emitting and receiving circuits, which makes it difficult to measure low values of the transfer impedance between the two small electrodes. The double-dipole layout, as used by *Koons et al.* [1974], avoids this particular difficulty, but others may arise if, for instance, the two dipoles are not perfectly balanced electrically. *Pottelette* [1973] has discussed antenna systems in which the four electrodes are well separated from one another ; we prefer to call these quadripole layouts. Then, as he explained, it is advisable that the four electrodes be disposed along a straight line, so that the lines joining all possible pairs of emitting and receiving electrodes all subtend the same angle with the magnetic field, and therefore correspond to the same value of the LOR frequency ; two quadripole layouts of this kind are illustrated in Figure 10 of his paper. It did not seem possible to choose the best layout on purely theoretical grounds, so these two quadripole layouts, together with several of the double-monopole type, were tested comparatively in the course of the Porcupine experiments.

3. INSTRUMENTS

In point of fact, the CRPE instruments for the Porcupine experiments comprised two radio-frequency (RF) mutual-impedance probes : a high-frequency (HF) probe, working in the band 0.8 - 14.5 MHz, to measure electron density and temperature, and a medium-frequency (MF) probe, working in the band 0.1 - 1.5 MHz, to measure field-aligned drift velocity. Each probe consisted of a sensor and a set of electronics. The two probes used different sensors, but shared much of the main electronics, which was housed in the payload body. In this section, descriptions are given of the MF sensor, of the electronics, of the sequence of measurements that was made at MF, and of the calibrations that were performed in order to improve the accuracy ; the corresponding arrangements for the HF probe have been described elsewhere, though in less detail [*Häusler et al.*, 1981].

3.1. MF SENSOR

The MF sensor consisted of four similar units. Mechanically, each unit comprised an electrode in the form of a light-alloy sphere 3 cm in diameter, mounted on the end of an insulating support rod 1 cm in diameter and 7 cm long. This was mounted in turn on a small metal box which housed some miniature electronics. The connection from the electrode to the electronics was made by means of a very thin wire (diameter 10 μm) so as to minimize the capacitive coupling between this connecting wire and the plasma. A view of one such unit is given in Figure 3a.

Figure 3b shows a simplified circuit diagram of the unit, which had three functions : emission, reception, and measurement of the self-impedance of the electrode. In all cases, the electrode was biased permanently, with a steady potential of 10 V through a resistance of 10 MΩ, so as to draw an approximately constant current ($\sim$ 1 μA) of electrons from the plasma. In emission, moreover, the electrode injected into the plasma an alternating current varying in frequency from 0.1 to 1.5 MHz ; this current was applied to the electrode, through a capacitance of 0.2 pF, from a signal generator producing about 2 V rms. In reception, the variations of potential induced on the electrode were preamplified and passed on the main receiver ; the input capacitance of the preamplifier was about 0.5 pF. Finally, for measuring the self-impedance, the unit emitted and received simultaneously ; a

theoretical value of the self-impedance, in circumstances typical of the Porcupine experiments, is equivalent to a capacitance of 4 pF in parallel with a resistance of 0.2 MΩ. The functions of emission and reception were performed during the main cycles of scientific measurements, while the measurement of self-impedance was made less frequently, as part of the calibration cycle (see below).

The four units comprising the MF sensor were held away from the payload body on individual telescopic booms, deployed perpendicularly to the spin axis, so as to reduce the risk of perturbation (by the ion wake, for instance). For later reference, the units have been numbered from 1 to 4, starting at the tip of the payload. Different geometric arrangements of the units were adopted for the flight F2 and for the flights F3 and F4 ; the reasons for these differences will be explained later.

The arrangement used for the flight F2 is illustrated in Figure 4. On this initial flight, one of the aims of the MF mutual-impedance probe experiments was technical, namely to compare the respective merits of the double-dipole and quadripole layouts, as defined in § 2.2. Now it will be recalled that, in a quadripole layout, the four electrodes should be disposed along a straight line, because the LOR frequency depends on the angle between the transmission path and the magnetic field. In order for this angle to remain constant as the payload spins, the line in question should be parallel to the spin axis (unless the axis itself is parallel to the magnetic field). Such an arrangement was technically convenient because the four telescopic booms on which the MF sensor units were mounted could all have the same length. However, it required that the payload axis be inclined to the field. Also it has the disadvantage that it did not enable us to distinguish experimentally between the effects of field-aligned and of cross-field plasma drift (see § 2.1) ; we counted on being able to determine the cross-field drift velocity from the DC electric field measurements, and to make allowance theoretically for its effects on the MF probe. In conclusion, on Porcupine F2 the electrodes were spaced uniformly along a straight line about 2.4 m long, parallel to the payload axis ; thus the distance between adjacent electrodes was about 0.8 m. When the booms were fully deployed, the centre of each electrode was 1.5 m from the axis, and about 1 m from the surface of the payload. The angle between the payload axis and the magnetic field was nominally 30°, which corresponds to an LOR frequency of roughly half the

electron gyrofrequency ; this angle was maintained more or less constant during the flight, by means of an active attitude-control system. In azimuth, the payload was pointed approximately towards geographic north-east. Figure 4 represents the complete MF sensor on the F2 payload.

3.2. ELECTRONICS

The main electronic circuits were shared by the HF and MF probes. They occupied 12 modules, which were grouped together in a rack housed in the body of the payload. How the instrument worked may be understood by reference to the block diagram of Figure 5, which shows both the sensors and the electronics. The upper row of blocks represents the electronics for RF signal generation and emission, the middle row contains the instrument programmer and other logical devices, while the lower row represents the electronics involved in the reception. The receiver had a bandwidth of 20 kHz and a dynamic range of 56 dB. Its output, at a fixed intermediate frequency of 15 MHz, was handled by two separate detectors, one of which (the "high-level" detector) covered the upper half of the range, while the other (the "low-level" detector) covered the lower half. The relation between the RF input and DC output was quite closely linear for each of these two detectors throughout its 28 dB nominal working range ; their outputs are marked "HL" and "LL" respectively in Figure 5. These analog data went to the interface module, where they were converted into 8-bit numbers and passed on to the PCM telemetry.

These instruments repeated a pre-arranged program of operations, under the control of their internal programmer which was synchronized to the central programmer of the payload. A complete program lasted approximately 16 s (more exactly, 16 x 2048/1875 = 17.48 s), of which the first 14 and the 16 th were used for taking measurements, while the 15 th was used for calibrations. This program, which is illustrated in Figure 6a, was repeated without interruption as long as the instruments were working.

3.3. MEASUREMENTS

The measurements were made in cycles of approximately 2 s duration (more exactly, 2,18 s). The first half-cycle was devoted to active measurements, and the second half-cycle to passive measurements. The active measurements were the normal ones, in which a sinusoidal RF signal was trans-

mitted from one antenna, propagated through the plasma, and received on the other antenna, while the transmitter and receiver were swept in frequency together : the quantity measured was the modulus of the transfer-impedance function of the sensor formed by the two antennas. The passive measurements were similar, except that the transmitter was switched off, and the measurements were of the spectra of the noise received on a single antenna. Their main purpose was to detect any RF interference from the other experiments on board, particularly any narrow-band noise which could produce a spurious peak in the probe transfer function measured in the active mode of operation.

The measurement cycle is illustrated in Figure 6b. Throughout each cycle, the MF and HF probes operated during alternate periods, each of approximately 1/8 s duration (more exactly, 137 ms). During any one such period, the frequency was swept over the entire band, MF or HF as the case may have been.

The frequency-sweep was discontinous : in fact, the frequency was "stepped" rather than swept. The entire frequency band was covered in 256 discrete steps. These discontinuous frequency changes occurred at a rate of 1875 s^{-1}, determined by a clock signal from the central programmer that synchronized all the experiments in the payload. Thus each step, during which the frequency was more or less constant, lasted approximately 488 µs. The spacing of these steps in frequency was more or less uniform throughout the band, i.e. the sweep was approximately linear. However, the frequency that corresponded to each step was not predetermined exactly ; it was measured during each calibration cycle, and was assumed not to vary irregularly between any one calibration and the next.

Arrangements were made to change the connections from the transmitter and the receiver to the electrodes of the two probes in the course of the measurements. These arrangements were different for the MF and HF probes and, for each probe, were different for the active and passive half-cycles.

For the HF probe, the arrangements were fairly simple. The connections from the receiving dipole to the receiver were in fact fixed, while those from the transmitter to the transmitting dipole were interrupted during the passive half-cycle.

For the MF probe, the arrangements were relatively complicated. The connections from the transmitter and the receiver to the four electrodes of the MF probe were changed during each individual frequency-sweep, and also from each frequency-sweep to the next.

The changes that took place during each individual frequency-sweep were basically the same for the active and passive half-cycles. During each sweep, the connections from the transmitter and receiver to the four electrodes were interchanged between each frequency-step and the next : in other words, whichever electrodes were connected to the transmitter during any one step were connected to the receiver during the next, and vice versa. Thus the connections were interchanged 1875 times per second. During each complete sweep, 128 measurements were obtained with the transmission going in one direction, and another 128 measurements, interlaced with the former, were obtained with the transmission going in the opposite direction. The purpose of this rapid interchange of the roles of transmission and reception between the various electrodes was to detect any field-aligned drift motion of the plasma electrons and to measure its velocity, as was mentioned earlier. The auroral ionosphere is often highly irregular, so the properties of the plasma may vary rapidly along the trajectory of a rocket. Hence it was necessary to reverse the direction of transmission as rapidly as possible, namely between each frequency-step and the next, instead of making one complete frequency-sweep with the transmission in one direction, followed by another with the transmission in the opposite direction, which would have been easier technologically.

The connection changes that were made from each frequency-sweep to the next were different for the active and passive half-cycles ; they are represented symbolically in the upper part of Figure 6b. Here each set of four symbols placed one below another, in a vertical column, denotes the roles of the four electrodes. The uppermost symbol refers to the electrode nearest the front end of the payload, and the remaining symbols to the other

electrodes in their spatial order. Each electrode either emits (E), or receives (R), or is inactive (*). The two sets of four symbols associated with each sweep of the MF band represent the two sets of connections that existed at alternate steps in the frequency-sweep. The reasons why these various combinations of electrodes were chosen will be given later.

3.4. CALIBRATIONS

Because some of the effects sought for were small, notably the frequency-shift of the LOR, the measurements had to be made as precisely as possible, and a long series of calibrations was undertaken with this aim in mind. They were of three types, called "pre-flight", "external", and "internal" calibrations.

The pre-flight calibrations were performed in the laboratory, mostly with the help of an automatic calibrator built by the Centre National d'Etudes Spatiales at Toulouse. Among other things, they concerned the linearity of the response of the receiving system at various frequencies in the HF and MF bands, and also, for the flight F2 only, the degree of residual unbalance of the dipole emitting and receiving antennas of the MF probe in each of its two quadripole layouts (Figure 6b).

The external calibrations of the HF and MF probes involved standard passive 4-pole networks housed in two "calibration boxes", which were mounted in the payload but were separate from the main rack of electronic modules. So long as each sensor was stowed in the payload, its electrodes were connected, via spring contacts and screened cables, to one of these calibration networks. Thus in the laboratory, on the launching ramp, and for about 85 s after the launch, the probes measured known standard transfer functions during the parts of the experiment programme dedicated to active measurements. When the rocket entered the ionosphere and sensors were deployed, the connexions to the calibration networks were broken automatically ; then these external calibrations ceased, and were replaced by the normal active measurements of the unknown transfer functions of the sensors in the ambient plasma. The circuit diagram of the MF external calibration network, as used on the flight F2, is given in Figure 7.

The internal calibrations were made automatically in the first half of the last cycle of the experiment program (Figures 6a and 6c). This half-cycle contained four MF frequency-sweeps, during which the following quantities were measured : (1) the self-impedance Z_p of a dipole antenna formed by two adjacent electrodes of the MF sensor ; (2) the gain of the receiver in the MF band, measured from its input to both the low-level and high-level outputs ; (3) the MF transmitter frequency ; (4) a repeat of (3).

The frequencies were measured by a 12-bit binary counter, with an accuracy of ± 4 kHz for a single measurement. In practice the frequency of the transmitter, at any given step of its sweep, did not drift much throughout the period of one experiment program. Hence, in the post-flight analysis of the calibration data, it was possible to improve the accuracy by combining the data from a number of successive calibration cycles.

The main purpose of all the other calibrations was to ensure that sufficient data were obtained regarding the output from the transmitter and the sensitivity of the receiver that, in the post-flight data analysis, the probe transfer impedances measured in the plasma could be normalized by expressing them as ratios to the corresponding values in free space. For the MF probe, these values were calculated theoretically for each of the various electrical layouts of the sensor (Figure 6b). The measurements were only of the moduli of the transfer impedances, not of their phases.

4. PORCUPINE F2

4.1. TECHNICAL ASPECTS

The Aries rocket carrying the F2 payload was launched on the evening of 20 March 1977, at 19 h 22 m 0 s UT. The technical performance of the MF probe during the F2 experiment will now be described.

4.1.1. Calibrations

At the start of the recording of the PCM telemetry signals, the data refer to the calibrations that were made on the launching ramp and during the first 85 s after the launch. The external calibrations of the MF probe were performed satisfactorily, but their quality was worse than in the case of the HF probe, because the gain of the preamplifier in the sensor electronics was greater at MF, and consequently so was the receiver noise level : it was about 14 dB above the bottom of the dynamic range. The internal calibrations were correct also, with the exception of the dipole antenna self-impedance measurement, which failed due to break-through from the emission to the reception within the sensor electronics.

4.1.2. Sensor system

The deployment of the MF sensor system was only partly successful. According to the planned sequence of operations, the booms 1, 2 and 3 should have been deployed together 85 s after the launch, while boom 4 should have been deployed later, at 120 s. Direct checks on boom deployment were provided by telemetry signals from microswitches and potentiometers coupled to the deployment mechanisms, and also by examination of the remains of the payload, which were recovered after the flight [*Schmitt*, 1979]. Indirect checks were available from the MF signals received by the sensor units on the various booms. It is difficult to tell exactly what happened, since there are inconsistencies between the evidence from these two sources. Without going into the details we simply state our conclusions, which are that all four booms were deployed at the correct times, but that booms 1 and 2 were deployed to only part of their length, while booms 3 and 4 were deployed fully. Moreover, at about 142 s after launch, in the course of an operation by the payload attitude control system, some accident occurred that put the sensor unit on boom 3 completely out of action, both in emission and in reception. These failures were a severe set-back for the experiment.

4.1.3. Passive mode

Throughout the flight, measurements of the MF noise level were made regularly in the passive mode. It will be remembered, from § 3.3 and Figure 6, that in this mode on F2, the noise level was measured alternately between the sensor units 1 and 2 and between the units 3 and 4, while the received frequency was swept through the MB band. During a period of about 25 s after the deployment of boom 4, passive measurements of MF noise in the plasma were made more or less correctly, except for eventual errors due to the partial deployment of booms 1 and 2. In comparison with the levels observed before deployment, when the sensor units were connected to the external calibration box and thus practically grounded, there was a great enhancement of noise at low frequencies, below about 350 kHz. Here the noise level rose rapidly with decreasing frequency. At the lowest frequencies, this noise even saturated the output of the high-level channel. This additional noise was substantially stronger between sensor units 3 and 4 than between sensor units 1 and 2. For this reason it is thought to be of technological origin, and specifically due to interference from the telemetry system, the antennas for which are situated at the base of the payload. Fortunately, since the lower oblique resonance rarely occurred below 350 kHz in the present experiment, this technological noise was not a serious nuisance. Above 350 kHz, the noise level was similar for the two pairs of sensor units until the instant when unit 3 failed : thereafter, it was somewhat weaker in the layout **RR than in the layout RR**. It was more or less independent of frequency, and was only slightly higher than it had been previously when the electrodes of the sensor units were grounded through the external calibration circuit, with the exception of one or two spectral lines, at fixed frequencies, which are obviously technological. Besides these, some natural line emissions were detected ; this natural RF noise was observed in greater detail by the Berkeley free-flyer [*Carlson et al.*, 1977].

4.1.4. Active mode

We now turn to the performance of the instrument in its active mode of operation. Measurements of the MF signal levels were made in this mode for the four sensor layouts *ER*, E**R, EERR, and ERER, together, of course, with their complementary layouts *RE*, R**E, RREE and RERE respectively (see § 3.3 for the explanations of these terms).

Figure 8 shows the quick-look data from the high-level channel, concerning the measurements of these types made during the period 96-145 s after launch. This period included the first and second operations by the attitude control system, which spun the payload first at 2 t/s then up to 2.5 t/s ; the accident to sensor unit 3 occurred near the end of it. In the figure, the amplitude of the signal is plotted versus frequency, with thin lines for the four basic layouts and with thick lines for their complementary layouts ; the scales are linear.

In the pair of double-monopole layouts *ER* and *RE*, the data from which appear in the fourth column in Figure 8, the probe worked fairly satisfactorily up the moment when the sensor unit 3 went out of action : from then on, nothing at all was received in *ER*, and only noise in *RE*.

In the double-monopole layout R**E (third column in Figure 8), when nominally unit 4 was transmitting and unit 1 was receiving, no coherent signals were received, but the normal appearance of the noise, qualitatively similar to that received in the layout RR** in the passive mode (see Fig. 6), suggests that unit 1 was working correctly, which implies that the failure was of the emission from unit 4. In the complementary layout E**R, with unit 1 emitting, signals were received on unit 4 correctly, but they were much weaker than in the layout *ER*. Generally they lay in the low-level channel, and were difficult to distinguish from the noise. This general result can be understood as a consequence of the greater distance between the sensor units, three times that used in the previous pair of layouts.

The observation of such low transfer impedances indicates that the self-impedance of the payload body did not significantly perturb the measurement of transfer impedance in the double-monopole layouts ; the risk of such a perturbation was mooted in Section 2. The signal levels observed in the layout E**R place a limit on the self-impedance of the order of 1 % of the free-space transfer impedance between units 1 and 4, a limit which is surprisingly low.

In the quadripole layouts EERR and RREE (first column in Figure 8), resonances were observed with peak signal levels in the high-level channel, until the failure of sensor unit 3. Thereafter only much weaker resonances appeared, with peaks just above the bottom of the high-level channel, when units 1 and 2 were emitting. In the alternate periods when units 3 and 4 were supposed to be emitting, similar but weaker resonances were observed. The detection of signal in this layout RREE is inconsistent with the lack of signal in the layout R**E, unless the unit 4 were emitting just enough signal to be detected on the unit 2 but not on the unit 1.

The layouts ERER and RERE (second column in Figure 8) yielded the best resonances of all, and this throughout the entire period following the deployment of boom 4. Their highest peaks, which sometimes saturated the high-level channel, actually increased in amplitude when sensor unit 3 failed ; this finding is consistent with the theory of the probe.

From then on, taking also into account the failure of the emission on unit 4, the sensor layout alternated between ER*R and RE**. Clearly, in these layouts, the sensor system consisted essentially of units 1 and 2, with unit 4 playing a relatively minor role because of its remotences from unit 1. Unfortunately this role cannot be neglected, since it is potentially a source of non-reciprocity of the transfer functions measured in these layouts ; we shall return to this point in § 4.3.

After the failure of boom 3, the resonances observed in these layouts, nominally ERER and RERE, were well situated in the upper half of the dynamic range of the receiver. Figure 9 shows some the quick-look data for these two layouts, between 420 s and 470 s after launch ; the signals were similar to those observed with the layouts *ER* and *RE* just before the failure of boom 3 (see Column 4 of Figure 8), and they had the following characteristics :

- the average of the two resonance frequencies observed in the two complementary layouts, together with the average of the amplitudes of the two resonances, varied periodically with the period of the spin ;

- the LOR frequency-shift (i.e. the difference of the two resonance frequencies) also varied periodically ;

- the signal-to-noise ratio was less than expected, especially at low frequencies.

Despite these unfavourable circumstances, we have tried to extract scientific results from these data.

4.2. SCIENTIFIC RESULTS

4.2.1. Criteria for data selection

In trying to analyse the data got by the MF probe in its active mode, the first question that arose was one of priority. The data are voluminous, and are hard to interpret because of the uncertain geometry of the sensor system, so we have concentrated on just a few items that appear to be the most relevant to the objectives of our experiment. From Section 1, it will be recalled that the prime objective was to measure the velocity of the field-aligned drift motion of the thermal electrons, which should have revealed itself by causing the probe transfer function to be non-reciprocal, and in particular by causing the LOR frequency to shift whenever the direction of transmission between the two antennas of the probe was reversed. Hence we have given precedence to the unequivocal detection of this form of non-reciprocity.

This consideration enters first into the choice between the four sets of data corresponding to the different electrical layouts of the probe (see Figure 6), and specifically between the quadripole layouts (EERR or ERER) and the double-monopole layouts (E**R or *ER*). The quadripole layouts, involving balanced dipole antennas, have the theoretical advantage that their transfer functions are calculable precisely. But this advantage may be illusory in the present instance, because the sensor may well be perturbed as a result of its nearness to the payload body, or indeed because the electrode in each of its units is too near to the box housing the associated electronics. Moreover the quadripole layouts have one practical disadvantage, namely that unless the two dipoles are perfectly balanced electrically, a spurious frequency-shift arises if one or other dipole - or both - has a different degree of unbalance when emitting than when receiving. For the double-monopole layouts, the transfer functions may be less precisely calculable, because one is more or less obliged to assume that the RF potential of the payload body is zero. Before the Porcupine experiments, this

assumption was doubted, but some measurements made in the layout E**R and cited in § 4.1.4. above suggest that it is justified. The double-monopole layouts also have the distinct advantage for present purposes of offering no scope for any spurious frequency-shift to arise in the way just described. This fact is illustrated in Figure 8, where it is evident, between 125 s and 140 s after launch, that the two quadripole layouts (Columns 1 and 2) exhibit very strong frequency-shifts, which is not the case for the double-monopole layout *ER* (Column 4) ; however, when examining these data, we must bear in mind that they were recorded just after a freon release related to an attitude-control operation, and that the actual behaviour of the sensor unit 4 is unknown.

Accordingly we have concentrated on the following data :

- up to 142 s after launch, the data from the double-monopole layout *ER*/*RE* ;

- after 142 s, the data from the layout ERER/RERE, which we consider to have been working essentially as the double-monopole layout ER**/RE** (see § 4.1.4).

It will be recalled from § 4.1.2. that 142 s was the time at which the sensor unit 3 went out of action.

4.2.2. Data from the layout *ER*/*RE*

Unfortunately only 24 frequency-sweeps were recorded in this layout during the period from the deployment of sensor units 1-3 to the instant when unit 3 was damaged, and of these only 13 were exploitable.

Some of these sweeps showed no significant frequency-shift : Figure 10a gives an example. The ordinate is the ratio of the measured modulus of the transfer impedance Z_t to the modulus of its nominal value Z_v in a vacuum, i.e. to the value found theoretically assuming that the distance between the centres of the electrodes of sensor units 2 and 3 was 0.8 m (more exactly, 0.787 m), as it would have been had both these units been deployed correctly. The thin line represents data got with unit 2 emitting, and the thick line data with unit 3 emitting. Figure 10b shows the theoretical curve, calculated by the method of *Storey and Thiel* [1978] with the following assumptions : electron gyrofrequency

f_c = 1.34 MHz, as calculated from a magnetic-field model for the known position of the payload in space ; the angle β between the probe axis and the magnetic field, taken equal to the measured angle of 28.8° between the payload axis and the field (see Figure 4) ; no field-aligned drift of the thermal electrons. Strictly, this last assumption was that the field-aligned drift velocity was zero in the frame of the moving probe, but the frequency-shifts corresponding to drift speeds of the order of the speed of ascension of the payload (2.04 km/s) might not have been detectable. The theoretical curve was fitted to the experimental one by adjusting the plasma frequency f_p and the electron temperature T_e ; the best fit, judged by eye, was obtained with f_p = 4.75 MHz and T_e = 1600 K. It is difficult to compare these values with those measured by other instruments on board, because the properties of the ambient plasma were fluctuating rapidly at the time. The HF quadripole probe gave 2.7 MHz < f_p < 4.0 MHz, while the retarding-potential analyser gave 1100 K < T_e < 2100 K, according to K. Spenner and W. Ott [Private communication, 1978]. Thus the electron temperature inferred from our MF data is consistent with the other measurement, but the inferred electron density is slightly too high. This last finding is related to the discrepancy between the theoretical and observed signal amplitudes, mentioned at the end of § 4.1.

Other sweeps, such as of Figure 10c, showed a clear-cut shift in the LOR frequency, here amounting to 57 kHz. Our sign convention is that we count the shift Δf as positive if the LOR frequency was higher when the direction of transmission was towards the base of the payload, i.e. in the present instance, when sensor unit 2 was emitting and 3 was receiving. Figure 10d presents the corresponding theoretical curves, calculated as above, with the difference that here the field-aligned drift velocity of the thermal electrons is a third adjustable parameter. The best fit to the experimental data was obtained with a plasma frequency of 4.0 MHz, an electron temperature of 1600 K, and a drift velocity of 33.6 km/s directed downwards ; the other parameters, determined as above, were f_c = 1.335 MHz and β = 28.8°. Note that, according to the theory, the resonance peak that is shifted towards the lower frequencies should increase in amplitude with respect to the other, which is confirmed by the data ; this was not always the case, however.

Taken with the electron density of 1.4×10^{11} m^{-3}, corresponding to the plasma frequency of 3.4 ($\pm$ 0.6) MHz measured by the HF probe, the drift velocity just quoted corresponds to a field-aligned current density of 7.7×10^{-4} A/m^2, which somewhat exceeds the highest value ever reported previously [*Anderson and Vondrak*, 1975]. This might be held to cast doubt on the soundness of the method of measurement. But considering that our method is the first to offer a truly local measurement, and that the velocities that it indicates vary greatly from one sweep to the next (2.18 s later), our results might nevertheless be regarded as compatible with the previous ones which, being derived from magnetometer data, necessarily had a poorer spatial resolution. Hence our first interpretation of our results was that they had revealed an irregular system of intense field-aligned currents.

Unfortunately this interpretation has proved to be untenable, for several reasons. Firstly, the experimental data from some of the frequency-sweeps agree worse with the theory than do those of Figure 10. Secondly, the results appear to show upgoing and downcoming currents close to one another in space. Rationales for these anomalies might perhaps be found. But the crucial evidence against our first interpretation of our data is that the observed LOR frequency-shifts depend on the spin-phase angle ϕ of the payload. Figure 11 shows how ϕ is defined. It is zero when the booms are directed upwards rather than downwards, and lie in plane containing $\mathbf{B_o}$ and the payload axis. If the payload is viewed along its axis looking towards the tip, then the spin is perceived as having a right-handed (clockwise) sense, and this sense of rotation corresponds to steadily increasing values of ϕ. In Figure 12, all the frequency-shifts Δf measured in the *ER*/*RE* layout are plotted against this angle, after normalization with respect to the local gyrofrequency f_c. A clear-cut dependence emerges : the variation of Δf as a function of ϕ looks roughly sinusoidal, and if the data points are smoothed by passing a sinusoid through them, its zeros occur near 0° and 180°, while its positive and negative peaks are near 90° and 270° respectively.

4.2.3. Data from the layout ERER/RERE

Similar behaviour is observed in the much larger set of data got in the layout ERER/RERE, after the failure of sensor unit 3. It will be remembered from § 4.1.4. that, with unit 3 out of action and unit 4 partially so, the signal transfer must have been occurring mainly between units 1 and 2, so the layout was effectively a double monopole in this case also. Figure 13 presents the data on the normalized frequency-shift $\Delta f/f_c$. Firstly, in the part (a), this quantity is plotted against the time after launch, and the data are disordered. Secondly, in part (b), it is plotted against the spin-phase angle ϕ, which orders them quite well. Again there is a periodic variation, very roughly sinusoidal. The maximum and minimum of Δf occur at about the same values of ϕ as in Figure 12, but here the fit to the data points is improved significantly if the sinusoid is offset towards positive values of Δf, so its two zeros are separated by less than 180°. A least-squares fit of an offset sinusoid of the form

$$\Delta f = \Delta f_o + \Delta f_1 \sin\phi \qquad (2)$$

to the data of Figure 13b leads to the results $\Delta f_1 \simeq 0.04\ f_c$ for the amplitude of the spin-dependent component of Δf, and $\Delta f_o \simeq 0.015\ f_c$ for the spin-independent component.

Though the latter component might perhaps have been caused by field-aligned drift, we cannot reasonably affirm this until we have succeeded in explaining the spin-dependent component, which must be spurious. The most striking fact about these spin-dependent frequency-shifts is that they are greatest in absolute value near $\phi = 90°$ and $\phi = 270°$. Interpreted in terms of electron drift motion, they correspond to motion upwards on one side of the payload and downwards on the other, which is absurd. The existing theory of the MF probe suggests no way in which such behaviour could have arisen. If the sensor axis (i.e. the straight line on which the four electrodes were supposed to lie) was parallel to the payload axis, then the spin motion would simply have transported the sensor system around the payload without altering the angle between the sensor axis and the magnetic field, and so - in the theory - without affecting the transfer function. If the four electrodes had not lain on a straight line, as would have been the case had not all of the booms been fully deployed, then the

directions of the lines joining certain pairs of electrodes would have varied as the payload spun, and these variations would have affected the value of the LOR frequency ; later we shall search for evidence of such effects in the data. But even if there had been distinct differences in length between the four booms, leading to a cyclic variation of the average LOR frequency, this should not have been accompanied by a relative shift of the frequencies measured for the two opposite directions of transmission. The spurious frequency-shifts must have been produced in some other way, and it is most important that their mode of origin be identified, in order that they may be eliminated in future experiments of the same type.

To help in the identification, it is interesting to examine how the frequency-shifts varied throughout the flight. For this purpose, the major variations related to the payload spin must be eliminated somehow. The following procedure was adopted : every five consecutive values of Δf, measured in the layout ERER/RERE, were plotted against the angle ϕ ; an offset sinusoid of the form (2) was fitted to these five data points by least squares ; the offset Δf_o, which is the spin-independent part of Δf, and the amplitude Δf_1 of the sinusoid representing the spin-dependent part, were assigned the time corresponding to the central point of the five. Then the values of these two parameters, for every set of five points, were normalized with respect to the electron gyrofrequency f_c and plotted against the time after launch (Figure 14). If their variations turned out to be correlated with those of any of the physical quantities measured by the other experiments on board, this fact might lead to identification of the origin of these spurious frequency-shifts.

Other data that might be useful in this respect include the average of the frequencies of the resonances observed in the two complementary layouts, the average of the amplitudes of the two resonances, and the difference of their amplitudes. These data will be presented later, as and when they may be needed.

4.3. INTERPRETATION

In seeking an explanation of the observed frequency-shifts, the following possibilities were studied :

- perturbation of the thermal plasma by the payload body ;
- perturbation of the suprathermal electron population by the payload body ;
- intrinsic non-reciprocity of the sensor due to electromagnetic effects ;
- technological defects of the sensor.

The mechanisms envisaged are described below.

4.3.1. Thermal plasma perturbation

It is natural to begin by examining the possible effects of plasma inhomogeneity due to perturbation by the body of the payload. The strongest perturbation is the reduction of the electron and ion densities in the wake, which extends outwards from the body in the direction of the velocity vector of the plasma relative to the payload. Since the trajectory was almost vertical, the wake should have been below the body on the upleg and above it on the downleg. Actually the direction of the wake is determined not only by the orbital velocity of the vehicle, but also by the velocity of the cross-field plasma drift due to the ambient electric field. In the present instance, our calculations were based on the electric field measured by R. Grabowski and H. Wolf [Private communication, 1978] ; the possible influence of field-aligned drift motion of the plasma *ions* was ignored in these calculations, though there is some evidence of the existence of such motion in the RPA data [*Spenner et al.*, 1979]. Figure 15a presents the temporal variations of the azimuth of the wake, this quantity being defined as the value of the angle ϕ at which the sensor is in the middle of the wake. Had there been no electric field in the plasma, had the earth's magnetic field been vertical instead of being inclined at 13° to the vertical, and had the trajectory been strictly vertical as well, then the azimuth would have been 180° on the upleg and 0° on the downleg. These considerations explain the general shape of the dashed curve in Figure 15a, which represents

the azimuth of the wake calculated using the true trajectory, but without taking the effect of the electric field into account. However, when this effect is included, the calculated azimuth remains within ± 30° of zero during most of the flight (solid line). Other properties of the plasma drift velocity relative to the payload are presented in Figures 15b and 15c. Figure 15b shows the modulus of its projection into the plane perpendicular to the payload axis, while Figure 15c shows the component parallel to this axis. From a comparison of these data with those of Figure 14, the drift velocity does not appear to be correlated in any way with the observed frequency-shifts.

Other conceivable strong perturbations caused by the body include the obstruction of field-aligned currents, and the collection of slightly supra-thermal electrons, i.e. those with energies greater than the potential of the body, but with gyro-radii distinctly less than its radius (0.5 m) ; both these perturbations should have been localized in the regions of space formed by the projections of the payload body up and down the magnetic field lines, which likewise were almost vertical.

Thus a feature common to the various perturbations mentioned above is that they should have been strongest in the regions more or less directly above and/or below the payload, so any effects that they might have had on the probe are expected to have been most marked when the sensor was within or nearest to one of these perturbed regions, and hence around the values of 0° and 180° of the spin-phase angle ϕ (see Figure 11). But Figures 12 and 13 show that the opposite is the case : the largest positive and negative shifts occur near 90° and 270° respectively.

At these positions, by the side of the body of the payload, the perturbations of the thermal plasma are expected to be weaker, but to be appreciable none the less. This fact is easiest to understand by considering initially the case where the plasma is stationary with respect to the payload. Then at any point in the plasma, outside the sheath a few Debye lengths thick that surrounds the body, the plasma is quasi-neutral in the sense that the electron and ion densities are almost exactly equal. But the ion density is less than it would be in the absence of the body, which intercepts some of the thermal ions that otherwise would pass by the point in question. If the ion trajectories can be approximated by straight lines, then the relative reduction in ion density is equal to the solid angle subtended by the body at that point, divided by 4π ; this factor attains its maximum

value close to the surface, this value being 0.5 if the whole of the surface is convex outwards. In order to preserve neutrality, the electron density is reduced to the same extent, and this implies that the plasma potential at the point must be negative with respect to its value far from the body on the same magnetic line of force : the relation between the potential V and the density N is

$$V = (kT_e/e)\ \ln(N/N_o) \tag{3}$$

$$\simeq (kT_e/e)\ \Delta N/N_o \qquad \text{if} \quad \Delta N/N_o \ll 1 \tag{4}$$

where k is Boltzmann's constant, T_e is the electron temperature of the plasma, e is the modulus of the electronic charge, $\Delta N = N - N_o$ is the change in electron density (a negative quantity), and N_o is the unperturbed density far from the body. ΔN, and hence V, become more negative as the body is approached, so it follows that there is an electric field in the plasma directed towards the body. In the presence of the earth's magnetic field $\mathbf{B_o}$ this electric field $\mathbf{E} = -\nabla V$ imparts a drift velocity $(\mathbf{E} \times \mathbf{B_o})/B_o^2$ to the thermal electrons. The resulting velocity field takes the form of a circulation of electrons around the body, the sense of the circulation being clockwise when viewed in the direction parallel to the magnetic field. These perturbations of plasma density and potential, of electric field, and of electron drift velocity extend out into the plasma to distances of the order of the linear dimensions of the body. Since, in the present instance, the payload diameter is 1 m, these perturbations would be significant in the neighbourhood of the sensor units, which are at 1 m from the surface.

Now we turn to the case where the plasma as a whole is moving with respect to the payload. The main effects of the bulk motion are to distort the region of perturbed plasma, compressing it on the upstream side of the body and stretching it out on the downstream side ; the latter effect constitutes the wake. The importance of these effects depends on the ratio of the bulk plasma velocity to the random thermal velocity of the ions. When this ratio is distinctly less than unity, the wake is not very strongly developed. Then a quasi-neutral plasma perturbation persists all around the body, associated with a clockwise circulation of the thermal electrons, as described in the previous paragraph.

By the process outlined in Section 2, the cross-field drift velocity of the thermal electrons may be expected to produce a non-reciprocal frequency-shift Δf of the LOR as observed by the probe. Consideration of how Δf should vary as a function of the spin-phase angle ϕ reveals that it should vanish at $\phi = 0$ and 180°, because in these positions the vector $\mathbf{E} \times \mathbf{B}_o$ is perpendicular to the axis of the sensor, assuming that $\mathbf{E}$ is directed towards the payload body. Conversely, we would expect $|\Delta f|$ to have maxima at or near $\phi = 90°$ and 270°, as indeed is observed. However, rough theoretical estimates of the magnitude of $|\Delta f|$ lead to maximum values much smaller than are observed. Also the theoretical sign of Δf is incorrect : the predicted sign is negative at $\phi = 90°$ and positive at $\phi = 270°$, whereas the contrary is observed (see § 3.3). In a word, this process is unable to explain the observed spurious frequency-shifts.

4.3.2. Supra-thermal electron perturbation

The impossibility of explaining these spin-dependent frequency-shifts in terms of inhomogeneity in the spatial distribution of the thermal or slightly supra-thermal electrons directed our attention to the more strongly supra-thermal electrons, i.e. those having gyro-radii comparable with or greater than the radius of the payload body. Obviously any electrons that are capable both of influencing the sensor and of being perturbed by the payload body must be on trajectories that pass close to one of the sensor units and also intercept the body. Because the frequency-shifts are greatest when the booms are perpendicular to the magnetic field, it follows that the gyro-radii of the electrons concerned must be greater than half the distance of 1 m from the sensor to the body, which means that their energies must exceed about 50 eV. In the range 50–500 eV, most of the electrons encountered in the present experiment would have been auroral ; they included auroral primary electrons, reduced in energy after collisions with neutral atmospheric particles, and also secondary electrons arising from collisional ionisation [*Banks et al.*, 1974].

In examining how these supra-thermal electrons were perturbed by the payload body, we assume that their unperturbed fluxes were isotropic ; experimentally, this is usually the case, to within 20 % or so [*Sojka et al.*, 1976]. To begin with, we approximate the body by a cylinder with its axis parallel to the magnetic field $\mathbf{B}_o$, and we study the perturbation in a plane perpendicular to $\mathbf{B}_o$ passing through the mid-point of the

body, i.e. the point half-way along its axis ; we call this the *mid-plane*. Let $\mathbf{r}$ be the position vector of an arbitrary point in the mid-plane, with respect to the origin on the payload axis. By considering which electrons are absorbed by the body, we find that, at all such points, there is a net electron flux in the direction of the vector $\mathbf{r} \times \mathbf{B}_o$. In other words, the perturbation takes the form of a net *circulation* of supra-thermal electrons around the body, in a left-handed (counter-clockwise) sense with respect to the direction of the magnetic field. Additionally, at all points out of the mid-plane, there is a component of flux along the field, downwards above the mid-plane and upwards below it. These anisotropies of the distribution function are most marked for electrons having gyro-radii of the order of r/2, and pitch angles not too far from 90°. If the hypothetical cylinder is replaced by the true shape of the payload, tapering to a point at its upper end, then the levels at which the field-aligned component of the flux is directed downwards extend a little below the mid-plane. Finally, if the inclination of the payload axis to the magnetic field is taken into account, it can be seen to enhance this field-aligned component in fairly obvious ways, as a result of the increase in the area of the projection of the payload onto a plane perpendicular to the field. Nevertheless, with an inclination of 30°, it appears probable that the counter-clockwise circulation mentioned above is the main perturbation of the supra-thermal electron population near to the central pair of sensor units (n°s 2 and 3).

The effects of this perturbation on the transfer function of the MF probe are difficult to predict. Difficulty arises because the type of perturbation concerned, namely an energy-dependent anisotropy of the electron distribution function in the plane perpendicular to the magnetic field, could not occur if the plasma were uniform, so its influence on the dispersion equation of the electrostatic waves cannot be studied quantitatively without taking the non-uniformity into account. In order to make progress we have assumed, somewhat arbitrarily, that the effects are qualitatively similar to those that would occur in a uniform plasma, if it were moving as a whole across the magnetic field in the direction that we have inferred for the local flux of the supra-thermal electrons. This assumption reduces the problem to the one considered previously, concerning the effects of cross-field drift of the thermal plasma, to which we applied the arguments developed in § 2.1. and illustrated in Figure 2c. In the present context, they lead to the conclusion that the counter-clockwise circulation of electrons around

the payload body should give rise to a spin-dependent frequency shift Δf that is positive when $\phi = 90°$, negative when $\phi = 270°$, and vanishes when $\phi = 0°$ or $180°$. These findings agree with the data of Figure 12, which were got in the double-monopole layout, using only sensors 2 and 3. Similarly, in the data of Figure 13, the phase of the sinusoidal component of Δf as a function of ϕ is predicted correctly. Lastly, the negative sign of the spin-independent component Δf in the data of Figure 13 (see also Figure 14) agrees with the predicted effect of the field-aligned component of the supra-thermal electron flux, though this may be taking the argument too far. In sum, although we are unable to predict the magnitude of Δf, its dependence on ϕ is consistent with an explanation in terms of the supra-thermal electrons in the ambient plasma.

An attempt was made to confirm this explanation by seeing whether the LOR frequency-shift was correlated with the flux of supra-thermal electrons, as measured by the retarding potential analyzers [*Spenner et al.*, 1979]. Figure 16 shows the variations of the total flux of electrons with energies above about 4 eV. One notable feature of this flux was a reduction by a factor of 10 or so from about 160 s to about 240 s after the launch, in the altitude range 275-390 km on the upleg. Similar reductions were observed by the electrostatic analyzers, in the energy range 0.1-25 keV on the main payload [*Wilhelm*, 1980], and in the range 0.5-40 keV on the free-flying sub-payload [*Mallincdrodt and Carlson*, 1977] ; the data from the main payload are shown in Figure 17, and those from the free-flyer in Figure 18. However, no significant reduction in the frequency-shift occurred during this interval (see Figure 14), which rules out the possibility of its being caused by the natural supra-thermal electrons.

Another possible explanation, suggested by G. Haerendel [Private communication, 1977], is that the spin-dependent frequency-shifts might have been caused by photoelectrons emitted from the payload body ; again, their energies would have had to exceed about 50 eV in order for them to have been able to reach the sensor units. Their fluxes near to the sensor units are hard to estimate, but varied evidence suggests that they might have been comparable with those of the auroral electrons in the same range of energy [*Grard*, 1973]. However, if the previous argument concerning the phase of the sinusoidal component of the variation of Δf with ϕ is applied to the emission of photoelectrons from the body, the predicted phase is the opposite of that due to the collection of auroral electrons, so it conflicts with our data.

A further indication that photoelectrons from the payload body were not involved is the absence of any effects associated with the earth's shadow. The optical shadow was at an altitude of about 155 km during the flight, so the hard X-ray shadow was - at a guess - a little below 250 km. Neither on the upleg nor on the downleg did the amplitude of the sinusoidal component change significantly as this level was crossed (Figure 14).

4.3.3. Electromagnetic effects

Mention should now be made of an attempt to explain the spin-dependent frequency-shifts in a completely different way, in terms of an intrinsic non-reciprocity of the sensor system due to invalidity of the quasi-static hypothesis, on which the theory of *Storey and Thiel* [1978] was based. If this hypothesis is abandoned, then the theory allows there to be non-reciprocity even in a stationary magnetoplasma. This fact is exemplified by the Faraday effect in electromagnetic wave propagation, which is well known as a cause of non-reciprocity in ionospheric radio links [*Budden and Jull*, 1964]. It was conceivable that the non-reciprocal frequency-shifts observed by the MF probe might be caused by some short-range analogue of the Faraday effect.

What this effect amounts to is that, when calculating the transfer impedance between the two antennas that constitute the probe system, we should consider not only the electric field created by the charge on the electrode of the emitting antenna, but also the magnetic field created by the current in the connecting wire through which this charge is applied to the electrode ; similar considerations apply to the receiving antenna.

In order to illustrate briefly how this effect could lead to non-reciprocity in the MF experiment, let us take the simpler case of two small dipoles with vector electrical lengths $\mathbf{p}_1$ and $\mathbf{p}_2$ separated by a vector distance $\mathbf{r}$ in a stationary magnetoplasma ($r >> p_1, p_2$). For a given alternating current applied to the emitting dipole $\mathbf{p}_1$, the potential difference V_{12} induced on the receiving dipole $\mathbf{p}_2$ obeys the following law of proportionality :

$$V_{12} \propto \mathbf{p}_1 . \mathbf{G}(\mathbf{r},\omega) . \mathbf{p}_2 \qquad (5)$$

where $\mathbf{G}(\mathbf{r},\omega)$ is the inverse spatial Fourier transform of the tensor Green's

function of the plasma defined in Fourier space [*Quémada*, 1968]. Now, in the complementary layout where $\mathbf{p}_2$ emits, the potential difference received on $\mathbf{p}_1$ is, of course,

$$V_{21} \propto \mathbf{p}_2 . \mathbf{G}(\mathbf{r},\omega) . \mathbf{p}_1 \tag{6}$$

If the same current is being emitted, the factor of proportionality is the same as in (5). According to Onsager's relations [*Stix*, 1962], the quantities V_{12} and V_{21} are not necessarily equal. Their difference is of the form

$$V_{21} - V_{12} \propto \mathbf{g} . (\mathbf{p}_1 \times \mathbf{p}_2) \tag{7}$$

where $\mathbf{g}(\mathbf{r},\omega)$ is a vector lying in the plane defined by the magnetic field vector $\mathbf{B}_o$ and the distance vector $\mathbf{r}$. Clearly, if the two dipoles are parallel to one another then $V_{21} = V_{12}$, but if they are not parallel then $V_{21} \neq V_{12}$ in general, which means that the antenna system considered is non-reciprocal.

In extending this reasoning to the actual MF sensor system in a double-monopole layout, we argue that even though the booms that support the two sensor units are parallel to one another, the vector electrical lengths of the two monopole antennas are not so. The reason for this is that, besides the electrode on the sensor unit, each antenna makes use of a second electrode, namely the payload body. Hence its electrical length is the vector distance from the centre of the electrode on the sensor unit to the electrical centre of the body, and it follows that the vector electrical lengths $\mathbf{p}_1$ and $\mathbf{p}_2$ of the two antennas cannot be parallel.

However, the symmetry of the sensor system is such that both of these vectors must lie in the plane defined by the booms and by the payload axis ; thus their product $\mathbf{p}_1 \times \mathbf{p}_2$ is perpendicular to this plane. As the payload spins, this vector remains constant in magnitude but its direction rotates. The vector $\mathbf{g}$, on the other hand, remains constant in all respects. Consequently we have the following results :

- when the spin-phase angle ϕ (see Figure 11) is equal to 0° or to 180°, the vectors $\mathbf{g}$ and $\mathbf{p}_1 \times \mathbf{p}_2$ are mutually perpendicular, so $V_{21} = V_{12}$;

- when $\phi = 90°$, the vectors $\mathbf{g}$ and $\mathbf{p}_1 \times \mathbf{p}_2$ are coplanar and the quantity $V_{21} - V_{12}$ takes an extreme value, positive or negative ;

- when $\phi = 270°$, the direction of the vector $\mathbf{p}_1 \times \mathbf{p}_2$ is opposite to its direction when $\phi = 90°$, so $V_{21} - V_{12}$ takes another extreme value, equal in magnitude but *opposite in sign* to its value when $\phi = 90°$.

Thus, in a qualitative way, electromagnetic effects appear to be capable of producing a spurious non-reciprocity with a dependence on spin-phase angle similar to that which is observed.

However, a quantitative analysis, which will be published elsewhere, has disclosed that these effects, though real, are much too small to explain the observed frequency-shifts.

4.3.4. Technological defects

Having exhausted all the possibilities that had occurred to us for explaining these frequency-shifts in physical terms, finally we were led to envisage causes of a purely technological nature. An obvious possibility of this kind arises when a quadripole layout is being used, if one of the four units of which the sensor is composed has a fault such that it either emits but does not receive, or receives but does not emit. The sensor would then exhibit a spurious non-reciprocity. Now it will be recalled from § 4.1.4. that sensor unit 4 did indeed have a fault of this type : it failed to emit, or, at least, its emission was so weak as to be undetectable in the quadripole layout ERER/RERE, because of the failure of sensor unit 3. Obviously we should consider the likelihood that the non-reciprocity observed in this layout, as described in § 4.2.3. and illustrated by Figure 13, may be explicable in this way. However, although this mechanism offers a simple explanation of the existence of non-reciprocity, it does not, in itself, explain why the non-reciprocal LOR frequency-shifts should depend on the spin-phase angle. If the four electrodes were in line parallel to the axis of the payload, as they were intended to be, then the non-reciprocity due to the partial failure of sensor unit 4 should not have been affected by the spin. In order to explain the observed dependence on the spin-phase angle, it is necessary to suppose that at least one of the four booms was bent in such a way that the sensor unit mounted on it no longer lay in the plane defined by the other units and by the payload axis. By making an additional hypothesis of this type, it is possible to explain some - but not all - of the non-reciprocal behaviour of the probe in the layout ERER/RERE.

Figure 19 presents the results of an attempt to simulate this behaviour numerically, assuming a Maxwellian magnetoplasma with a gyrofrequency f_c = 1.3 MHz, a plasma frequency f_p = 2.3 MHz, and an electron temperature T_e = 2500 K, which are representative values for the F2 flight. On the left-hand side of the figure, all the data from the layout ERER/RERE concerning the amplitude and the frequency of the LOR, at times later than 142 s after the launch, are graphed against the spin-phase angle. On the right-hand side, similar graphs are shown of the theoretical values of the same parameters, which were calculated on the following hypotheses :

- the boom 1 was only partially deployed, to a length of 1.1 m instead of 1.5 m, as the boom monitor signals suggest [*Schmitt*, 1979] ;

- the boom 2 was deployed to 1 m only (which is compatible with the monitor signals) ;

- sensor unit 3 was out of action ;

- sensor unit 4 emitted but did not receive, and moreover boom 4 was bent in azimuth through an angle of 30° with respect to its nominal direction, the sense of this azimuthal displacement being clockwise when viewed in the direction parallel to the magnetic field (i.e. along the axis of the payload, towards its base).

The computed transfer impedances have had to be reduced in amplitude by a factor of 4, to allow for the discrepancy between the experimental and theoretical values that was mentioned previously in § 4.2.2. ; its possible causes will be discussed elsewhere.

On comparing the true with the simulated data, a general resemblance is seen. The variation of the average LOR frequency as a function of the spin-phase angle, which is due mainly to the difference in the assumed lengths of booms 1 and 2, is particularly well reproduced. The non-reciprocity, manifested as the differences between the two amplitudes and between the two frequencies observed in the two complementary layouts, is due to the behaviour of sensor unit 4. Most strikingly, the theoretical dependence of the LOR frequency-shift on the spin-phase angle is more or less as observed ; it was in order to obtain this agreement that the boom 4 was assumed to be bent. No doubt, by modifying the above hypotheses and perhaps by making some additional ones, the resemblance between the two sets of data could be made even better.

However, in view of the number of different hypotheses that could be made, and of the absence of any independent confirmation, we feel that this line of reasoning is not worth pursuing any further. Besides, similar non-reciprocal LOR frequency-shifts were observed in the layout *ER*/*RE*, as shown in Figure 12. Clearly the latter cannot be imputed to the failure of the emission from the sensor unit 4, which was not used in this layout, and since we are unable to explain them in terms of any other technical defect, we consider that some unidentified physical effect must have been responsible for them.

5. DISCUSSION

It remains to discuss the provisional conclusions that were drawn from the outcome of the Porcupine experiment F2. Since the spurious frequency-shifts prevented us from obtaining any geophysical results, our conclusions are concerned exclusively with the technology of the MF mutual-impedance probe, and in particular with how to get rid of these spurious shifts.

The first conclusion concerns the relative merits of the different possible electrical layouts of the sensor : the double-monopole layout appears preferable to the two quadripole layouts, for the following reasons. Firstly, the disadvantage that was anticipated in § 2.2., namely that the self-impedance of the payload body would contribute to the measured transfer impedance, does not appear to be significant, so it does not offset the advantage that this layout has by its relative simplicity. Secondly, if a sensor unit suffers a partial failure, whereby it emits but does not receive or vice versa, as happened to unit 4 on flight F2, then in a double-monopole layout the existence and the nature of this failure are apparent immediately, whereas in a quadripole layout it produces a spurious non-reciprocity, simulating the effects of field-aligned drift that we are looking for. These considerations led us to adopt the double-monopole layout for the flights F3 and F4.

On the flight F2, however, spurious frequency-shifts were observed even in a double-monopole layout, and although they have not been explained, the question arises as to how they might be reduced in future experiments. Fortunately, it is possible to suggest ways in which this might be done, even without knowing how these spurious shifts originate. It suffices to note that their spin-dependent component disappears whenever the sensor booms, the payload axis, and the earth's magnetic field are coplanar. Therefore the sensor system should be designed so as to ensure that this condition is satisfied permanently, regardless of spin phase. An example of a double-monopole system that meets this requirement is given in Figure 20 ; the payload axis is parallel to the magnetic field, while the two booms are of different lengths. With the dimensions shown in the figure, the angle between the sensor axis and the magnetic field is about 32°, which is a suitable value [*Storey and Thiel*, 1978]. If, by the use of such an arrangement, the spurious frequency-shifts could indeed be reduced greatly, then the frequency-shifts genuinely due to field-aligned electron drift might become detectable.

The arrangement shown in Figure 20 has another advantage compared to that used on the flight F2 (Figure 4), inasmuch as it enables a distinction to be made experimentally between the otherwise similar effects of field-aligned and of cross-field electron drift. The symmetry is such that an LOR frequency-shift due to field-aligned drift is independent of spin phase whereas any shift due to cross-field drift is modulated by the spin. This point was explained in § 2.2.

Accordingly the arrangement of Figure 20 was adopted as the basis of the design of the MF sensor for the flights F3 and F4. Further practical details of the improved sensor system will be given in the opening section of Part 2 of this report.

FIGURE CAPTIONS

1. Modulus of the potential ψ created by an alternating point charge in a warm magnetoplasma, at a fixed distance from the source :
(a) as a function of direction, at a fixed frequency, when the plasma is stationary ;
(b) the same function, when the electrons are drifting with a velocity parallel to the magnetic field $\mathbf{B_o}$;
(c) as a function of frequency, in two opposite directions (β = 30° and 150°), when the electrons are drifting.
For the values of the parameters, see the text.

2.(a) Illustrating how a change in the excitation frequency affects the resonance cones in a stationary magnetoplasma :
(1) situation at the initial frequency ;
(2) effect of lowering the frequency ;
(3) effect of raising the frequency.

(b) Illustrating how field-aligned drift affects the LOR frequencies observed in two opposite directions (dashed line) :
(1) effect of the drift at the initial frequency ;
(2) lowering the frequency brings one resonance cone into the upstream direction of observation ;
(3) raising the frequency brings the other resonance cone into the upstream direction of observation.

(c) Illustrating how cross-field drift affects the LOR frequencies observed in two opposite directions (dashed line) :
(1) effect of the drift at the initial frequency ;
(2) lowering the frequency brings one resonance cone into the downstream direction of observation ;
(3) increasing the frequency brings the other resonance cone into the upstream direction of observation.

3. One of the four units of the MF sensor :
(a) external view ;
(b) simplified circuit diagram.

4. Complete MF sensor mounted on the payload, in the arrangement used on the flight F2.

5. Instrument block diagram for the flight F2.

6. Experiment program for the flight F2 :
   (a) program outline ;
   (b) measurement cycle ;
   (c) calibration cycle.

7. Circuit diagram of the MF external calibration network. The standard capacitance associated with each pair of sensor units (1 and 4, or 2 and 3) was made up as follows : capacitance of each coaxial cable 120 pF ; lumped capacitance C inside the box 550 pF ; total 790 pF.

8. Quick-look data on the active MF measurements, from the high-level output of the receiver, between 96 and 145 s after launch. The four vertical columns correspond to the four different electrical layouts of the sensor.

9. Example of quick-look data on the active MF measurements in the layout ERER/RERE, from the high-level output, after the failure of sensor unit 3.

10. Examples of pairs of transfer functions measured on the flight F2 with the MF probe in the double-monopole layouts *ER* (thin line) and *RE* (thick line) :
    (a) pair showing no significant shift of LOR frequency (time after launch 132.92 s, altitude 222.83 km) ;
    (b) theoretical transfer function fitted to these data ;
    (c) pair similar to (a), but showing a frequency-shift (time after launch 128.55 s, altitude 213.85 km) ;
    (d) theoretical transfer functions fitted to these data.

11. Illustrating the definition of the spin-phase angle ϕ. The vertical dash-dot lines represent the direction of the earth's magnetic field.

12. Normalized LOR frequency-shift measured on the flight F2 in the double-monopole layout *ER*/*RE*, plotted against the spin-phase angle.

13. Normalized LOR frequency-shift measured on the flight F2 in the layout ERER/RERE, plotted against
(a) time after launch,
(b) spin-phase angle.
The dashed line in (b) is the best-fitting offset sinusoid of the form of Equation (2).

14. Variations during the flight F2 of the parameters characterizing the LOR frequency-shift observed in the layout ERER/RERE :
(a) the spin-independent part Δf_o, normalized with respect to the electron gyrofrequency f_c ;
(b) normalized amplitude Δf_1 of the spin-dependent part.

15. Variation during the flight F2 of the drift velocity $\mathbf{V}$ relative to the payload, calculated taking account of the orbital velocity of the payload and the electric field in the plane perpendicular to $\mathbf{B_o}$:
(a) azimuth of the component $\mathbf{V_\perp}$ in the plane perpendicular to the payload axis ;
(b) modulus of $\mathbf{V_\perp}$;
(c) component $V_{//}$ parallel to the payload axis.

16. Supra-thermal electron flux, after *Spenner et al.* [1979].

17. Electron number and energy fluxes, after *Wilhelm et al.* [1980].

18. Electron differential energy flux (upper panel), and plasmawave spectrogram (lower panel), after C.W. Carlson [Private communication, 1978].

19. Comparison of the experimentally observed (left column) and theoretically simulated (right column) properties of the LOR observed in the layout ERER/RERE :
(a) amplitude Z_o of the transfer impedance at the resonance, averaged for the two complementary layouts, and normalized with respect to its vacuum value Z_o ;
(b) difference ΔZ_o of the amplitudes for the two complementary layouts, normalized with respect to Z_o ;
(c) average resonance frequency f_o, normalized with respect to the electron gyrofrequency f_c ;
(d) frequency-shift Δf_o, normalized with respect to f_c.

20. Proposed double-monopole MF sensor system, for use on a payload with the spin axis oriented parallel to the magnetic field.

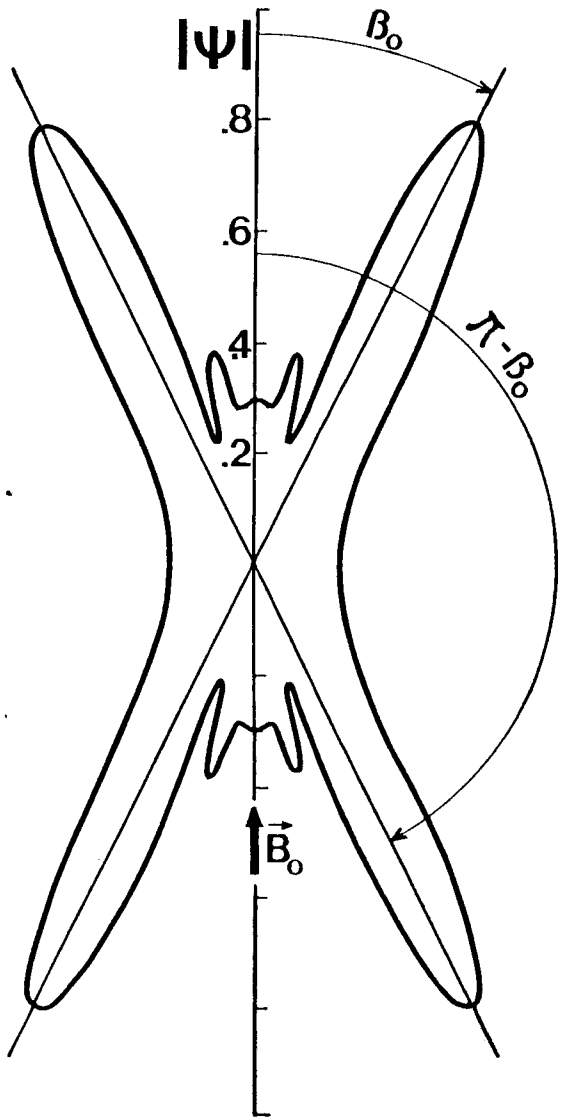

V=0

(a)

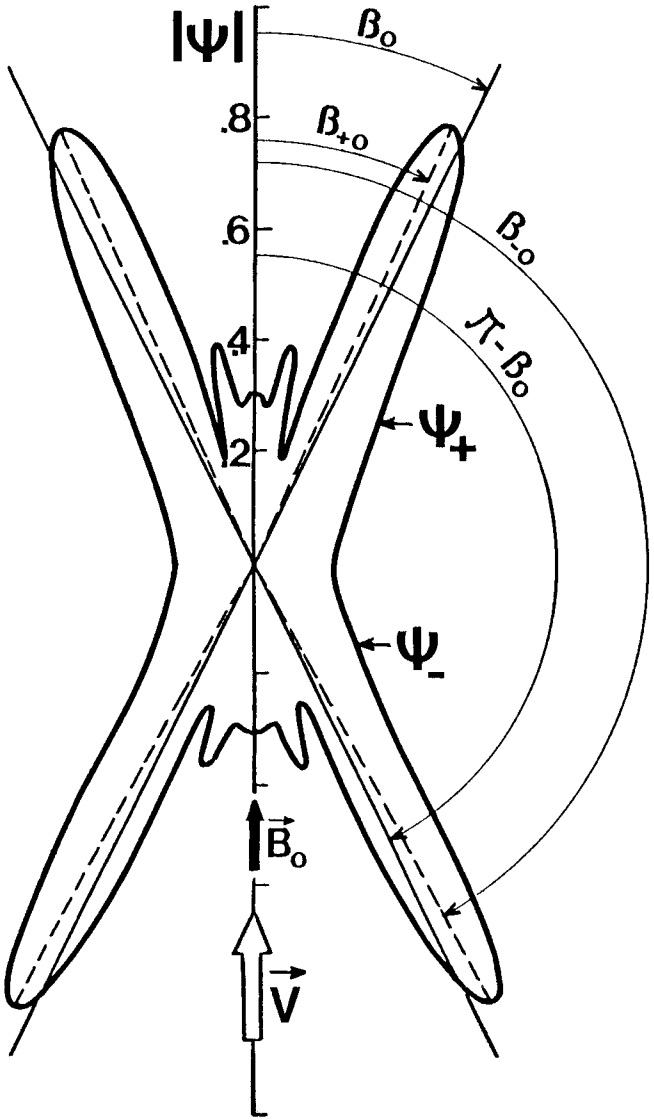

V = .16 V_{th}

(b)

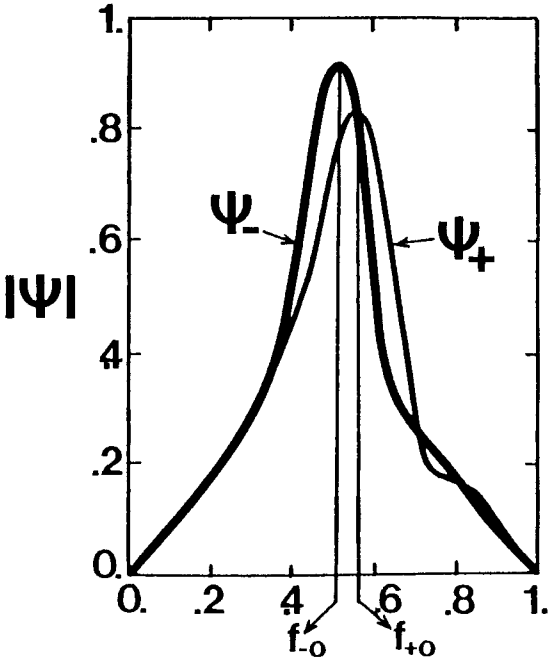

V = .16 V_{th}

(c)

FIGURE 1.

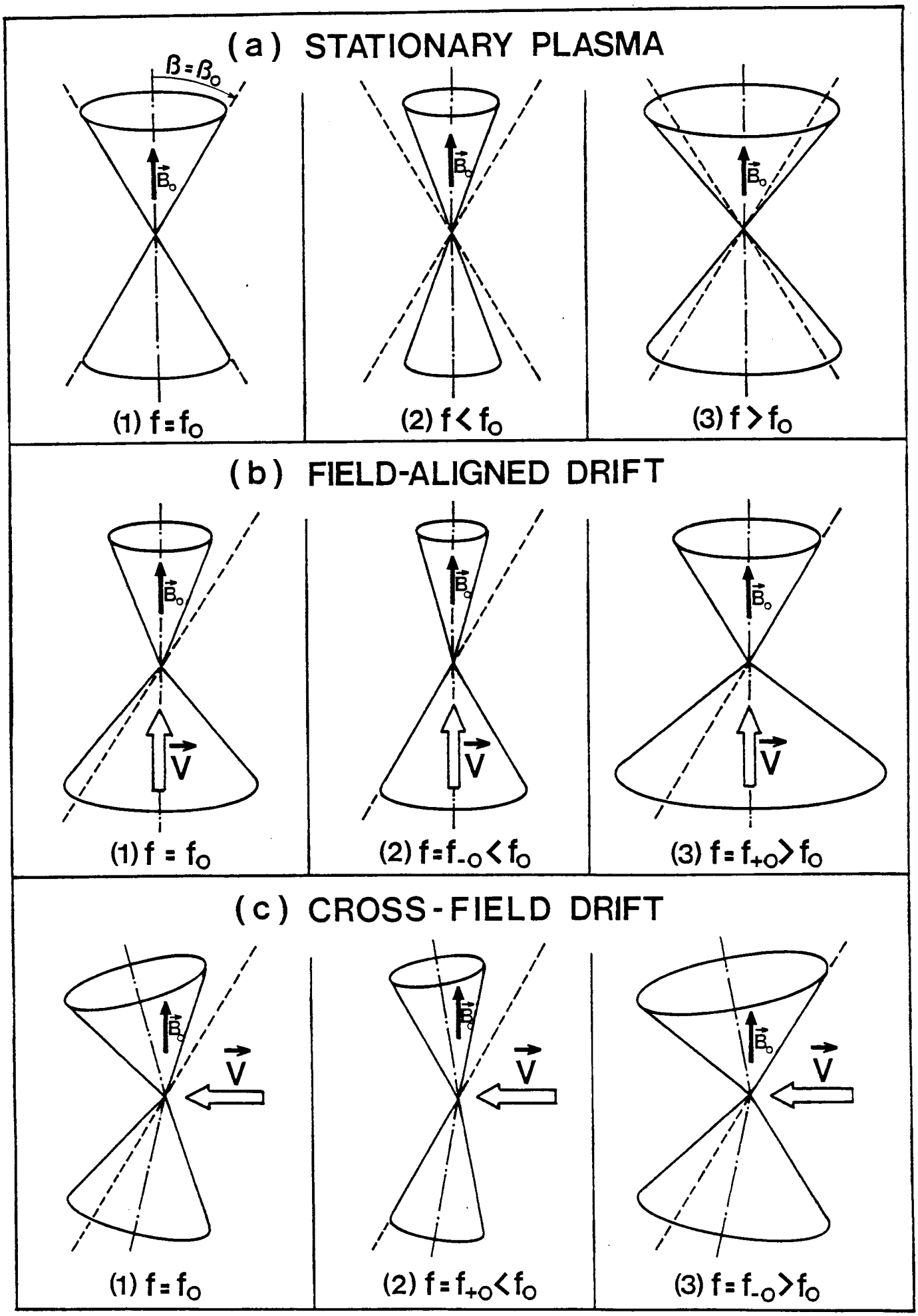
(a) STATIONARY PLASMA
β=β₀
B₀
(1) f=f₀
(2) f<f₀
(3) f>f₀
(b) FIELD-ALIGNED DRIFT
V
(1) f = f₀
(2) f=f₋₀<f₀
(3) f=f₊₀>f₀
(c) CROSS-FIELD DRIFT
(1) f=f₀
(2) f=f₊₀<f₀
(3) f=f₋₀>f₀

FIGURE 2.

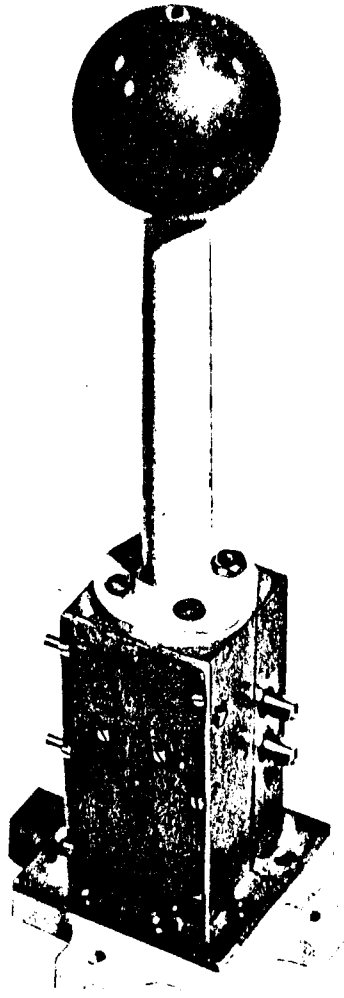

(a)

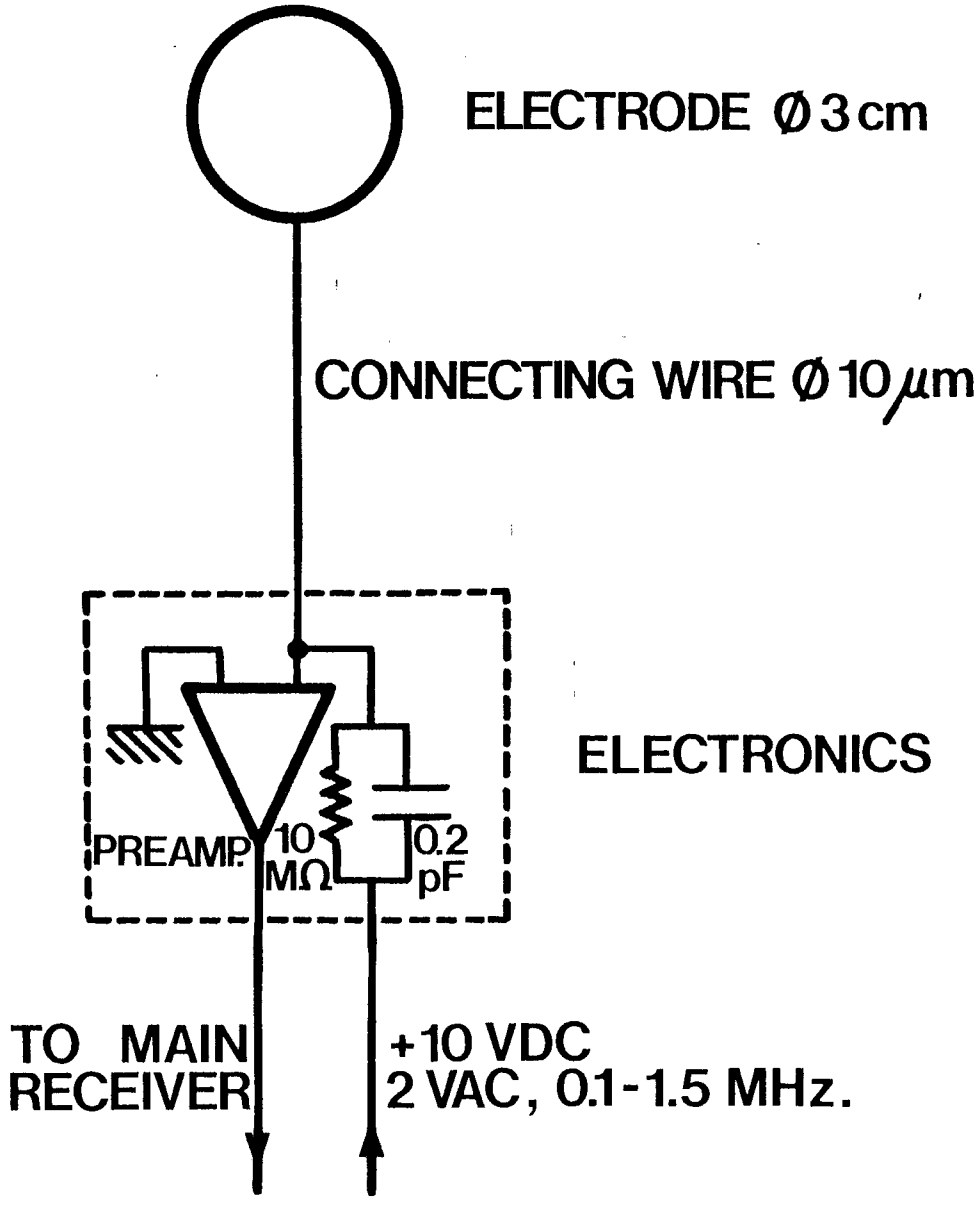
ELECTRODE Ø 3 cm
CONNECTING WIRE Ø 10 μm
ELECTRONICS
PREAMP.
10 MΩ
0.2 pF
TO MAIN RECEIVER
+10 VDC
2 VAC, 0.1-1.5 MHz.

(b)

FIGURE 3.

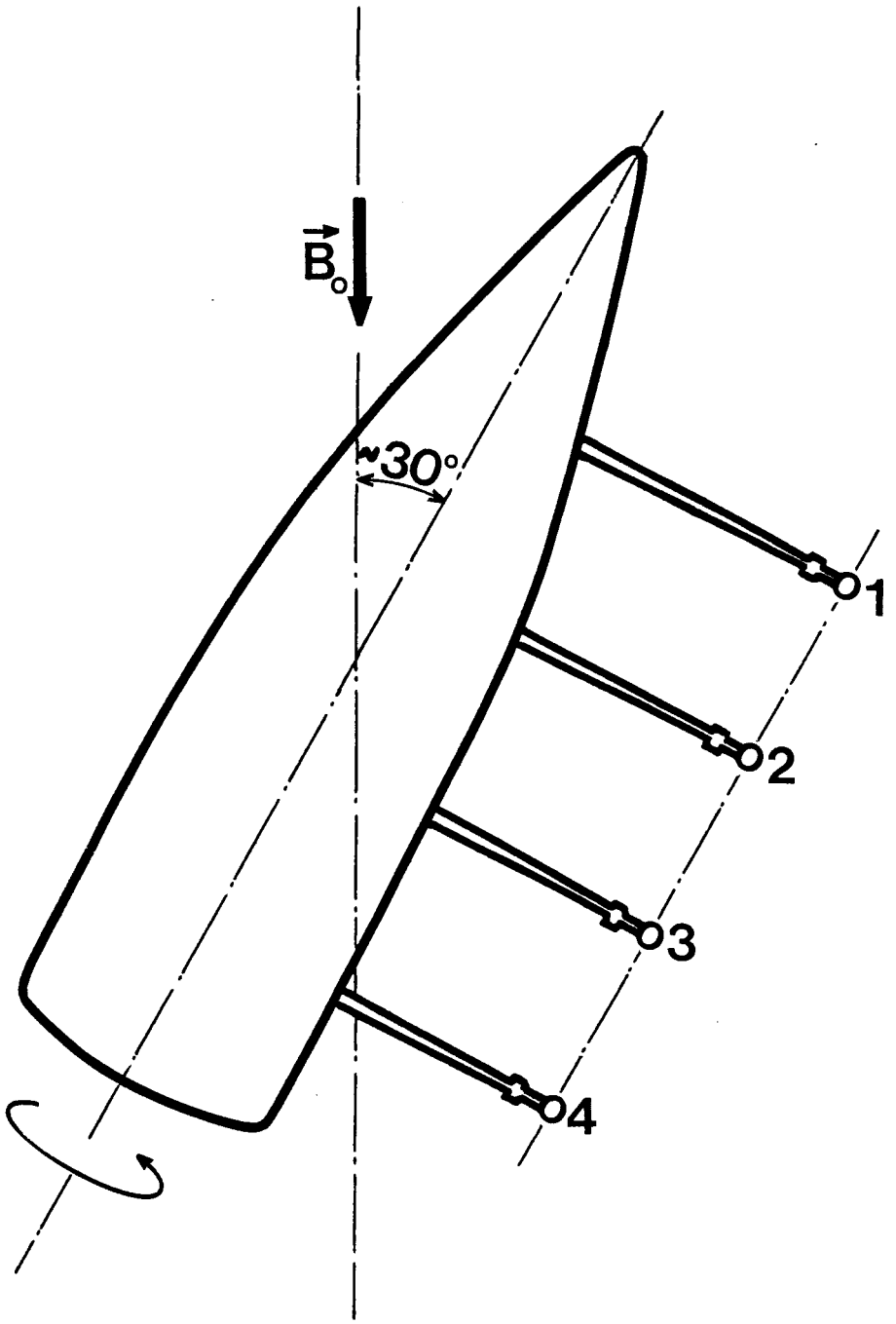

FIGURE 4.

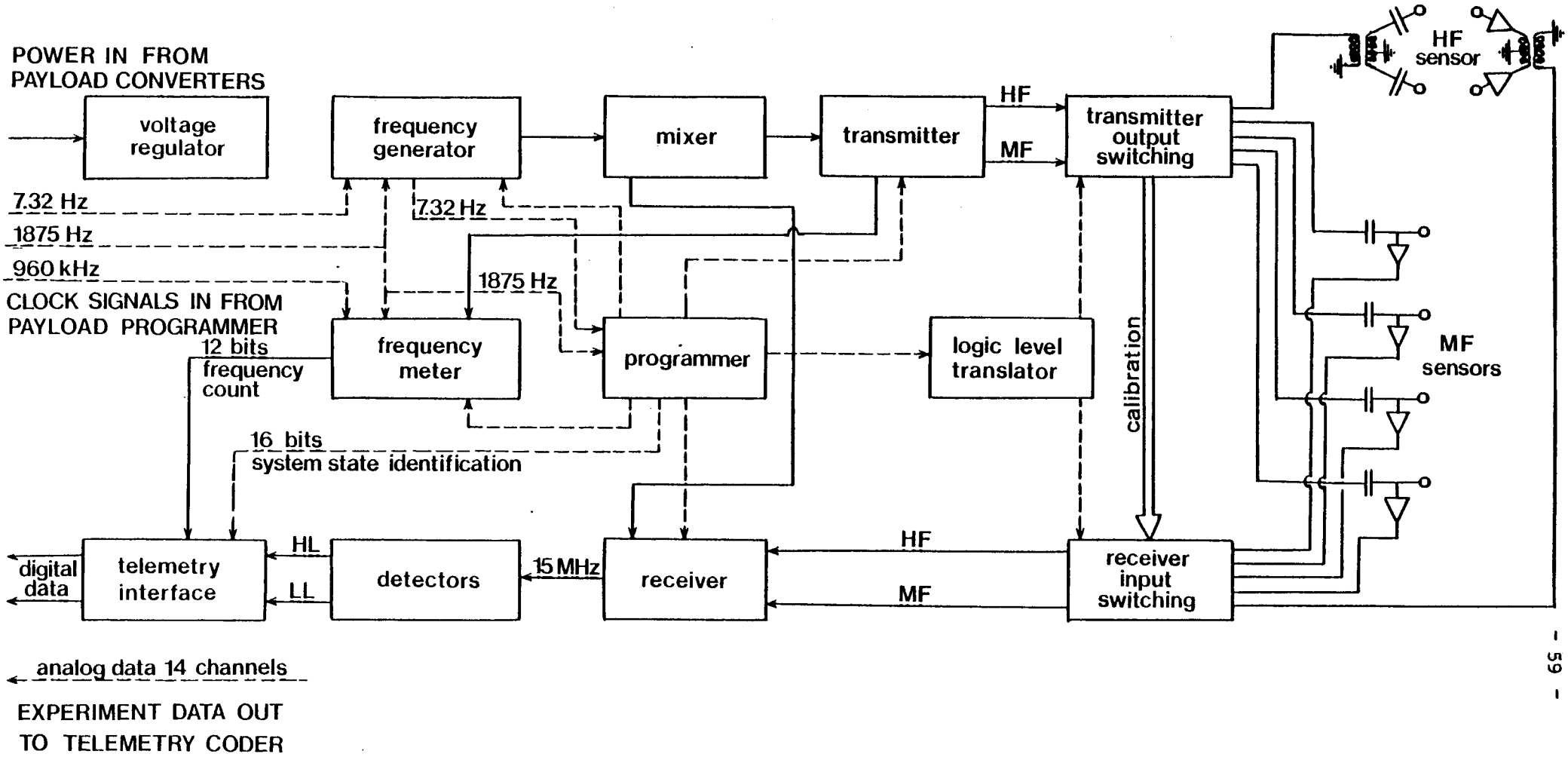
POWER IN FROM
PAYLOAD CONVERTERS
voltage regulator
frequency generator
mixer
transmitter
HF
MF
transmitter output switching
HF sensor
7.32 Hz
1875 Hz
960 kHz
CLOCK SIGNALS IN FROM
PAYLOAD PROGRAMMER
7.32 Hz
1875 Hz
12 bits
frequency count
frequency meter
programmer
logic level translator
calibration
MF sensors
16 bits
system state identification
digital data
telemetry interface
HL
LL
detectors
15 MHz
receiver
HF
MF
receiver input switching
analog data 14 channels
EXPERIMENT DATA OUT
TO TELEMETRY CODER

FIGURE 5.

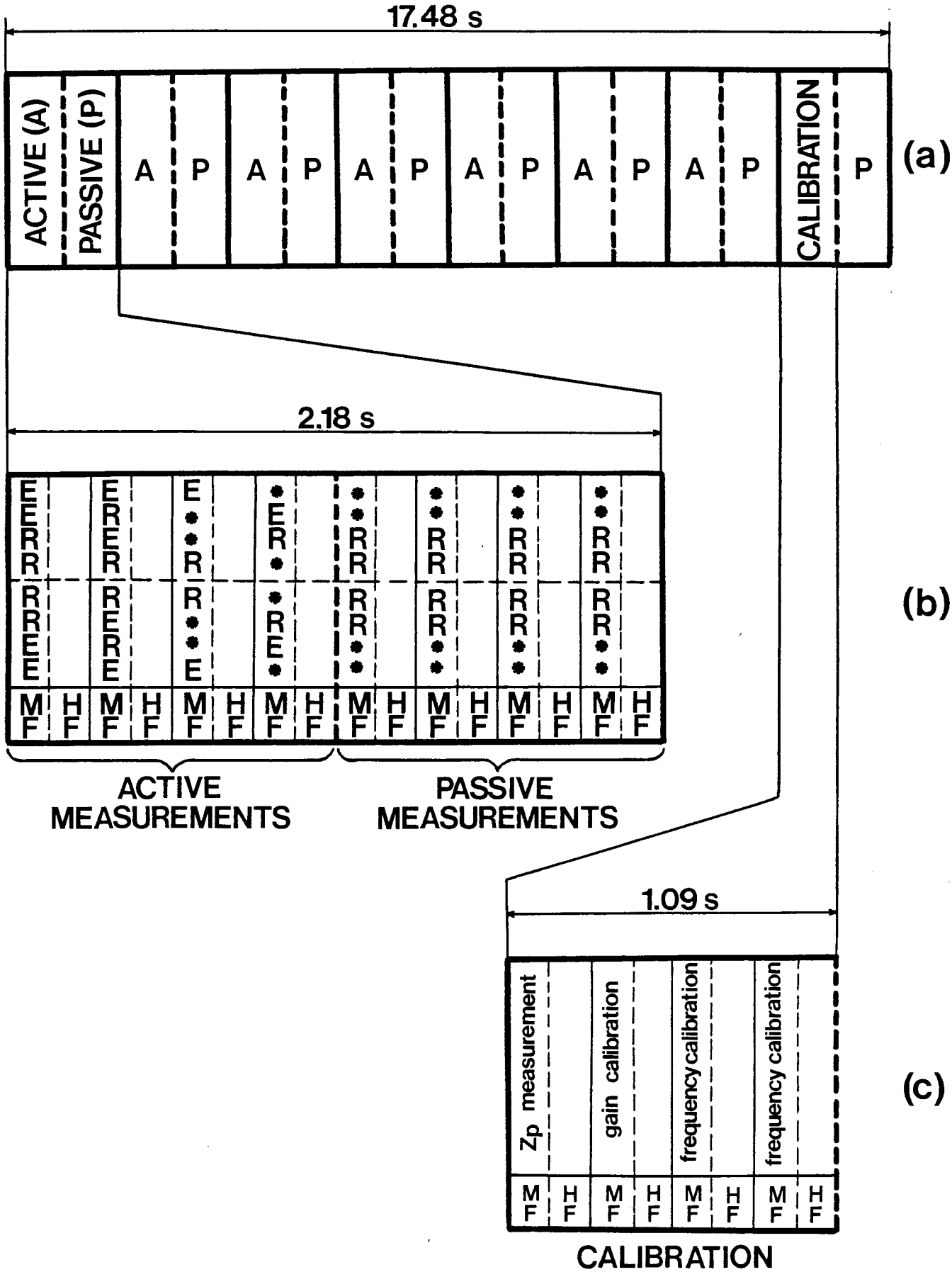
17.48 s
ACTIVE (A)
PASSIVE (P)
A
P
CALIBRATION
(a)
2.18 s
MF
HF
(b)
ACTIVE MEASUREMENTS
PASSIVE MEASUREMENTS
1.09 s
Zp measurement
gain calibration
frequency calibration
frequency calibration
(c)
CALIBRATION

FIGURE 6.

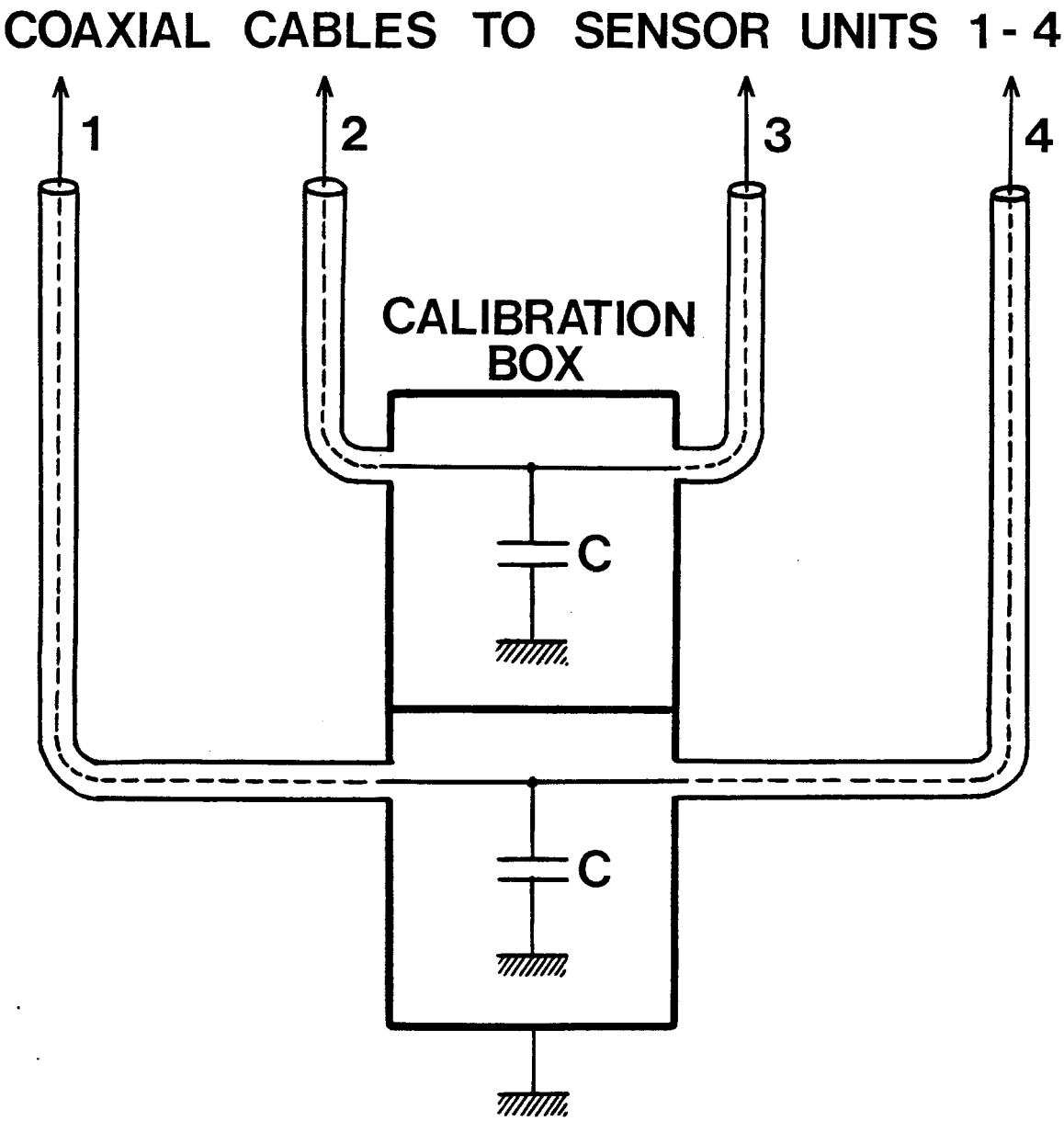

FIGURE 7.

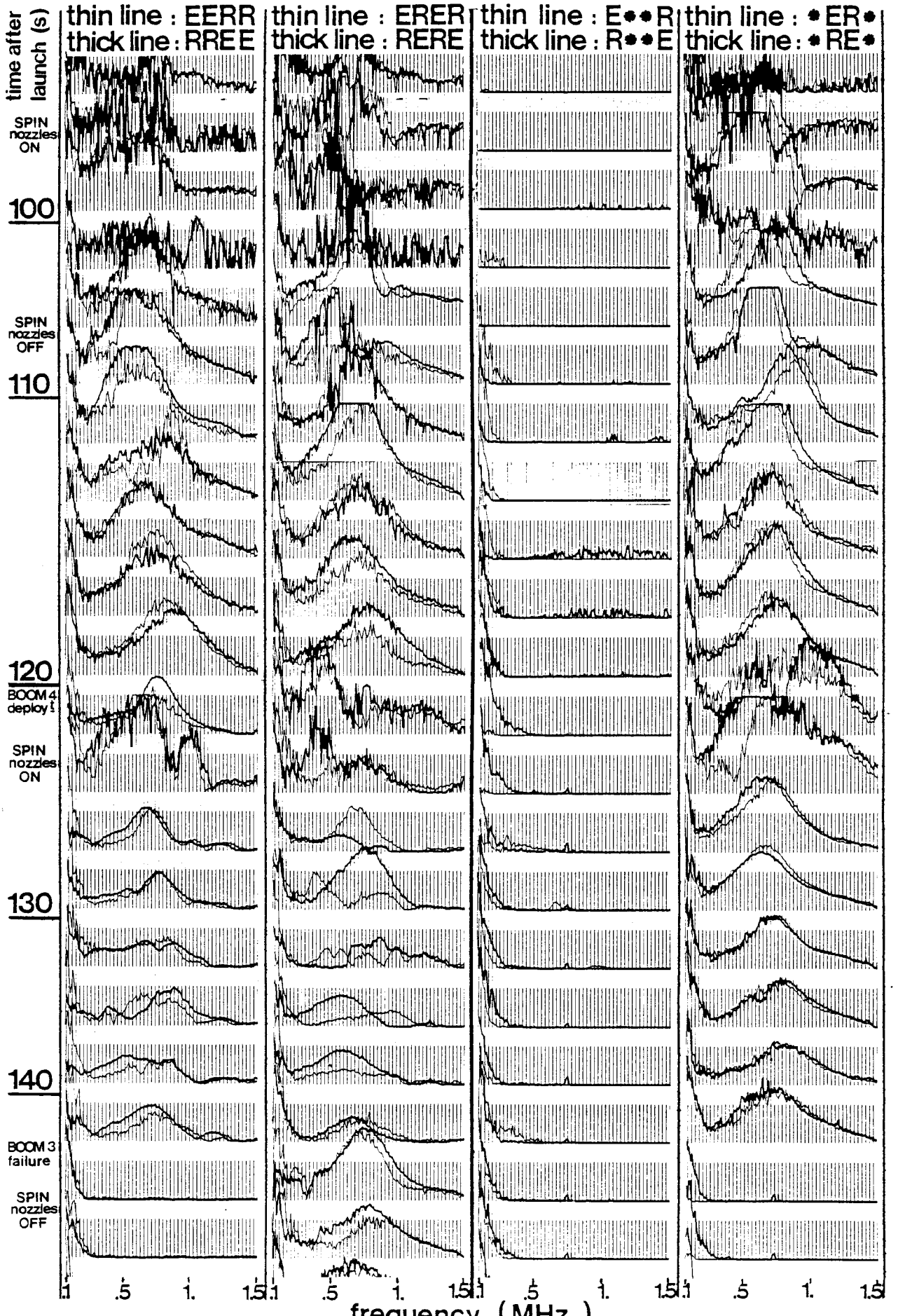
time after launch (s)
thin line : EERR
thick line : RREE
thin line : ERER
thick line : RERE
thin line : E••R
thick line : R••E
thin line : •ER•
thick line : •RE•
SPIN nozzles ON
100
SPIN nozzles OFF
110
120
BOOM 4 deploy
SPIN nozzles ON
130
140
BOOM 3 failure
SPIN nozzles OFF
.1
.5
1.
1.5
frequency (MHz.)

FIGURE 8.

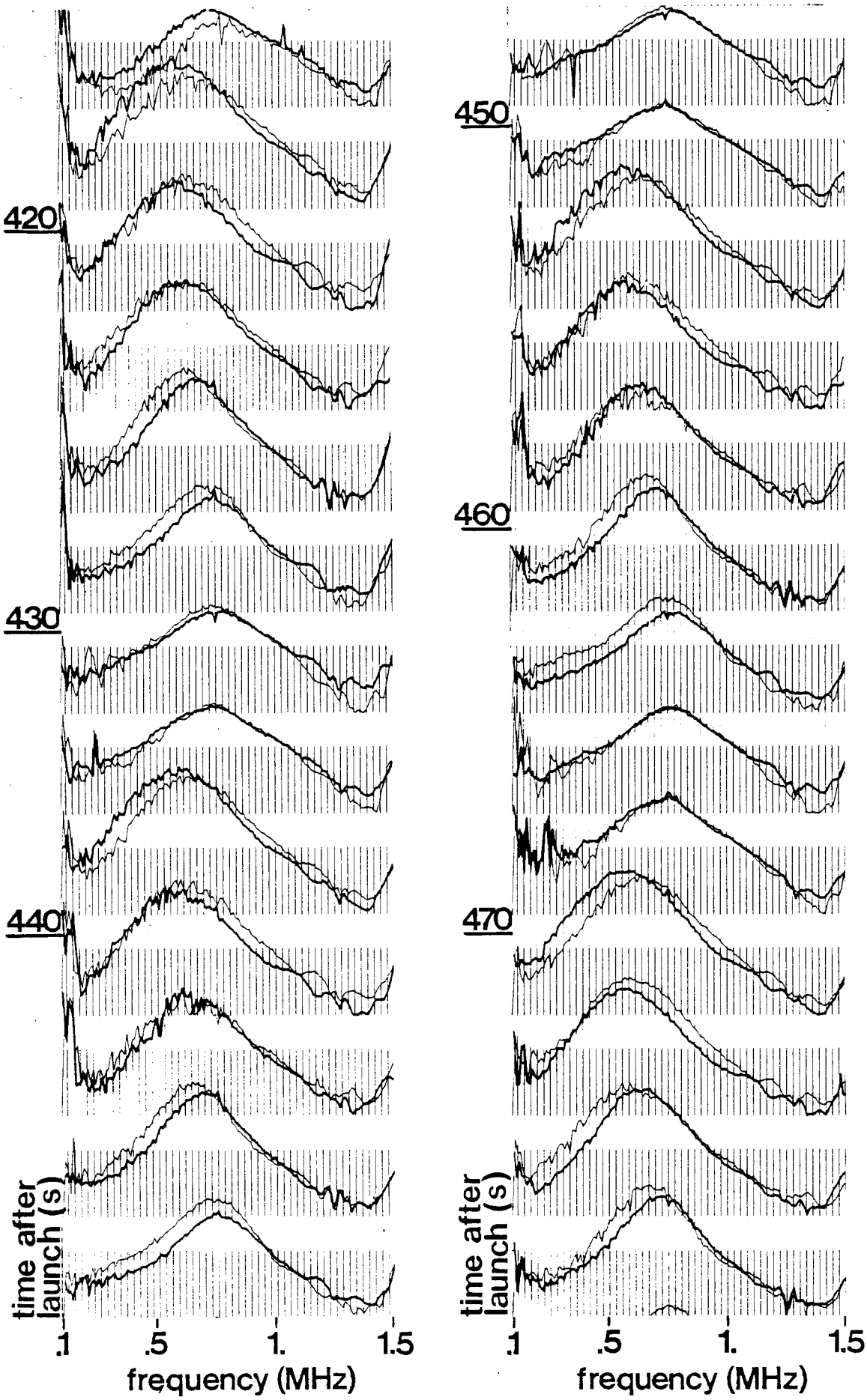
thin line : ERER - thick line : RERE
420
430
440
450
460
470
time after launch (s)
.1
.5
1.
1.5
frequency (MHz)

FIGURE 9.

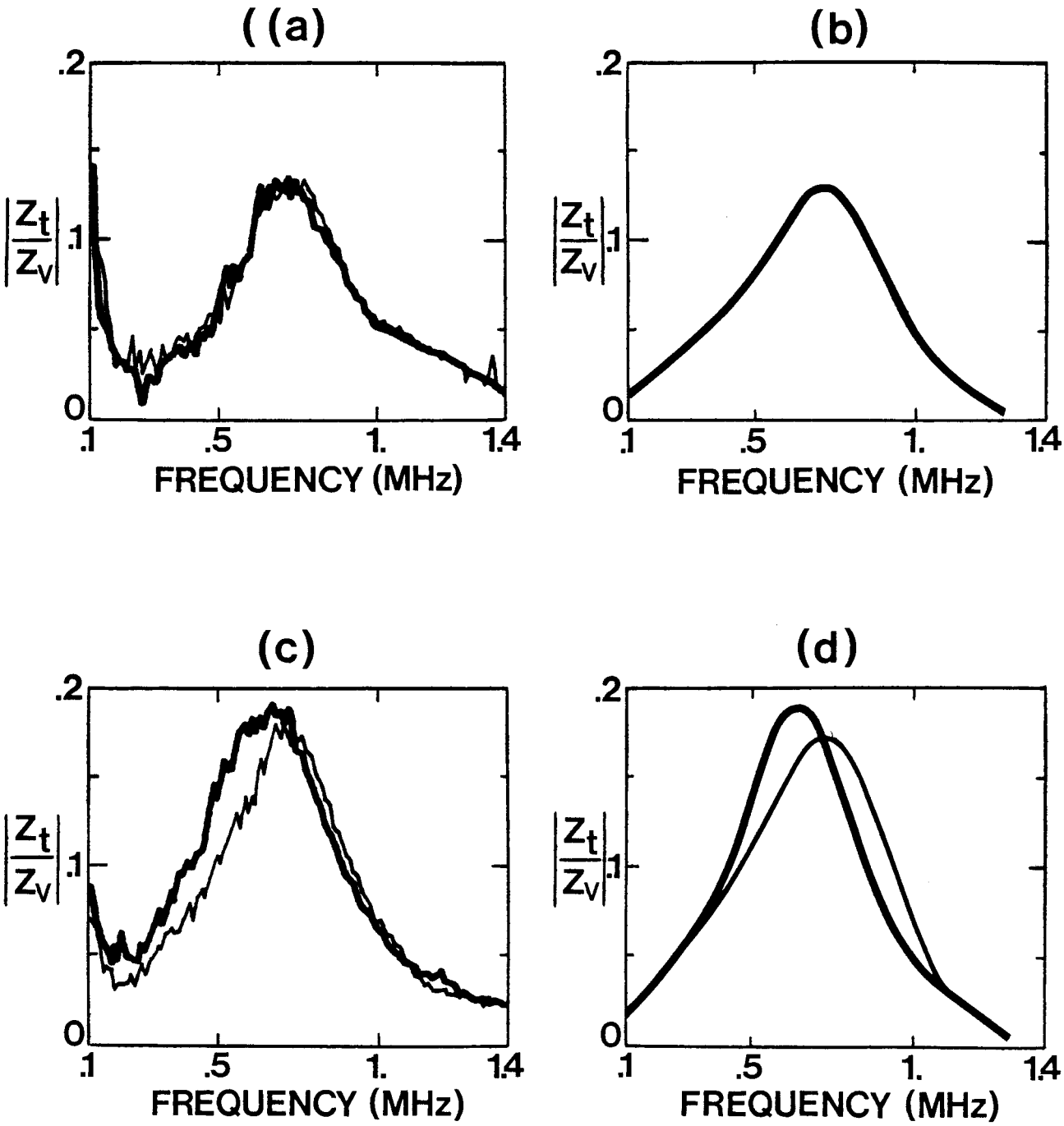

FIGURE 10.

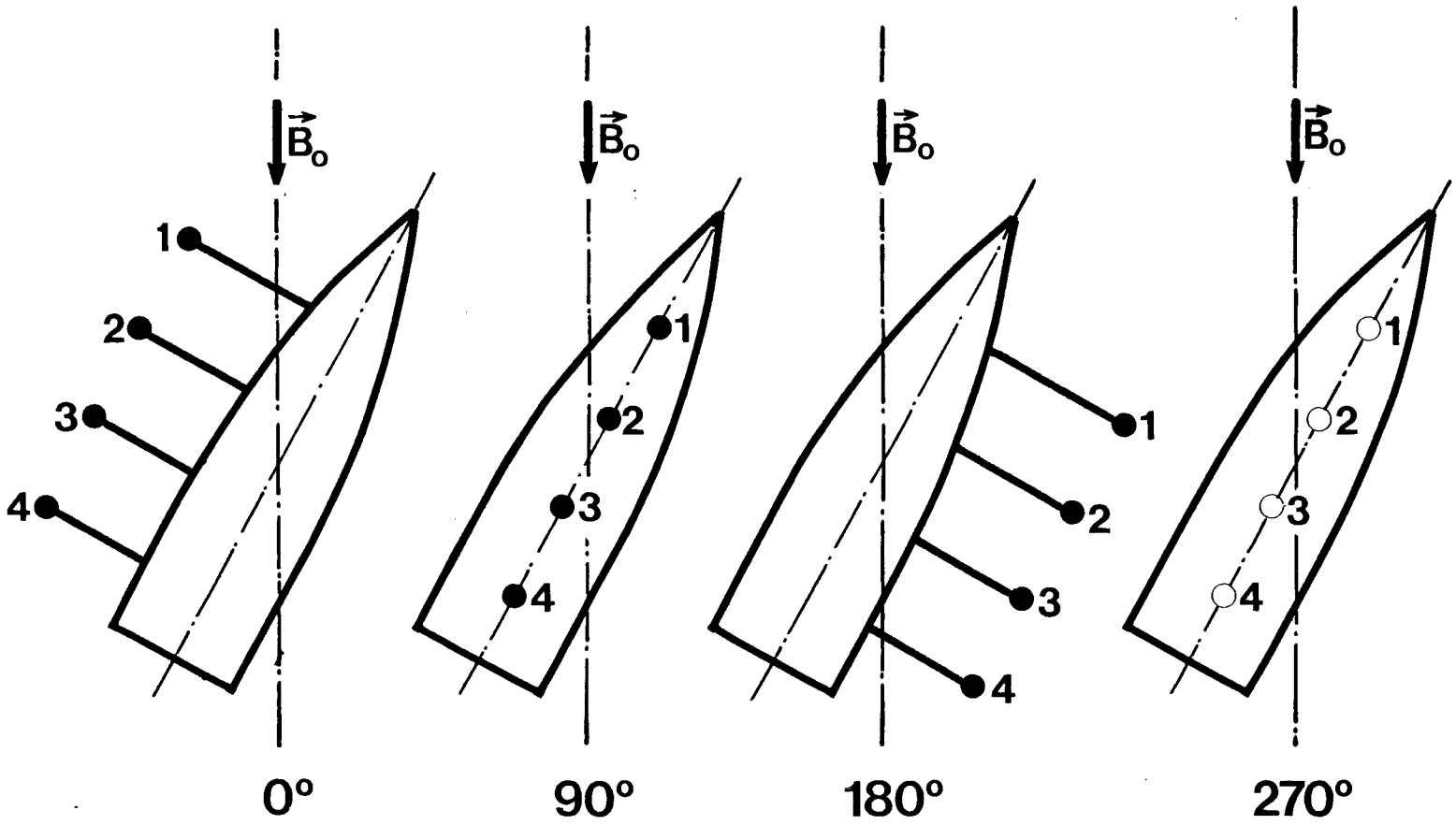

FIGURE 11.

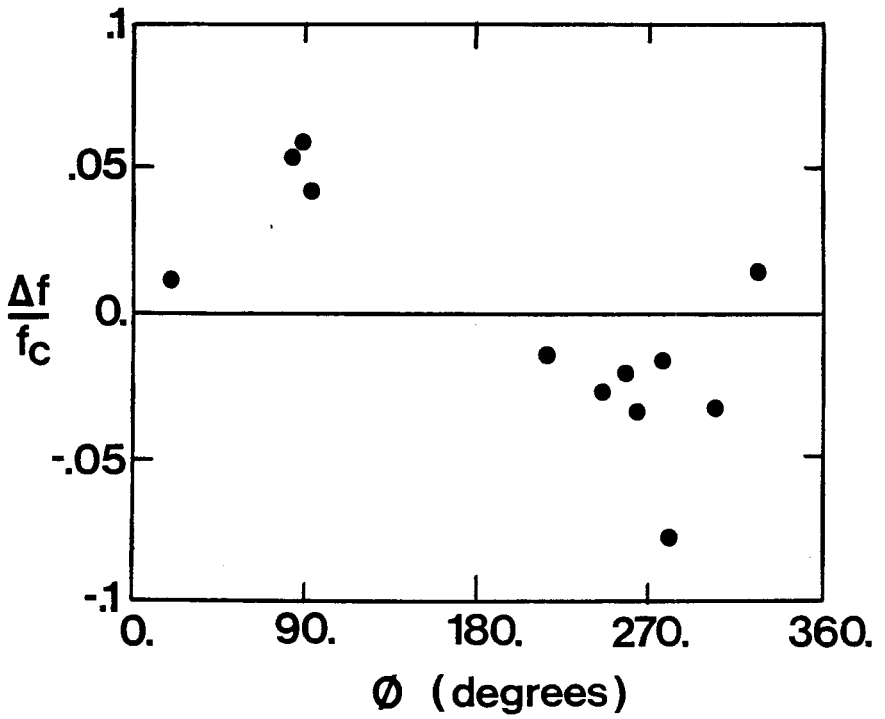

FIGURE 12 .

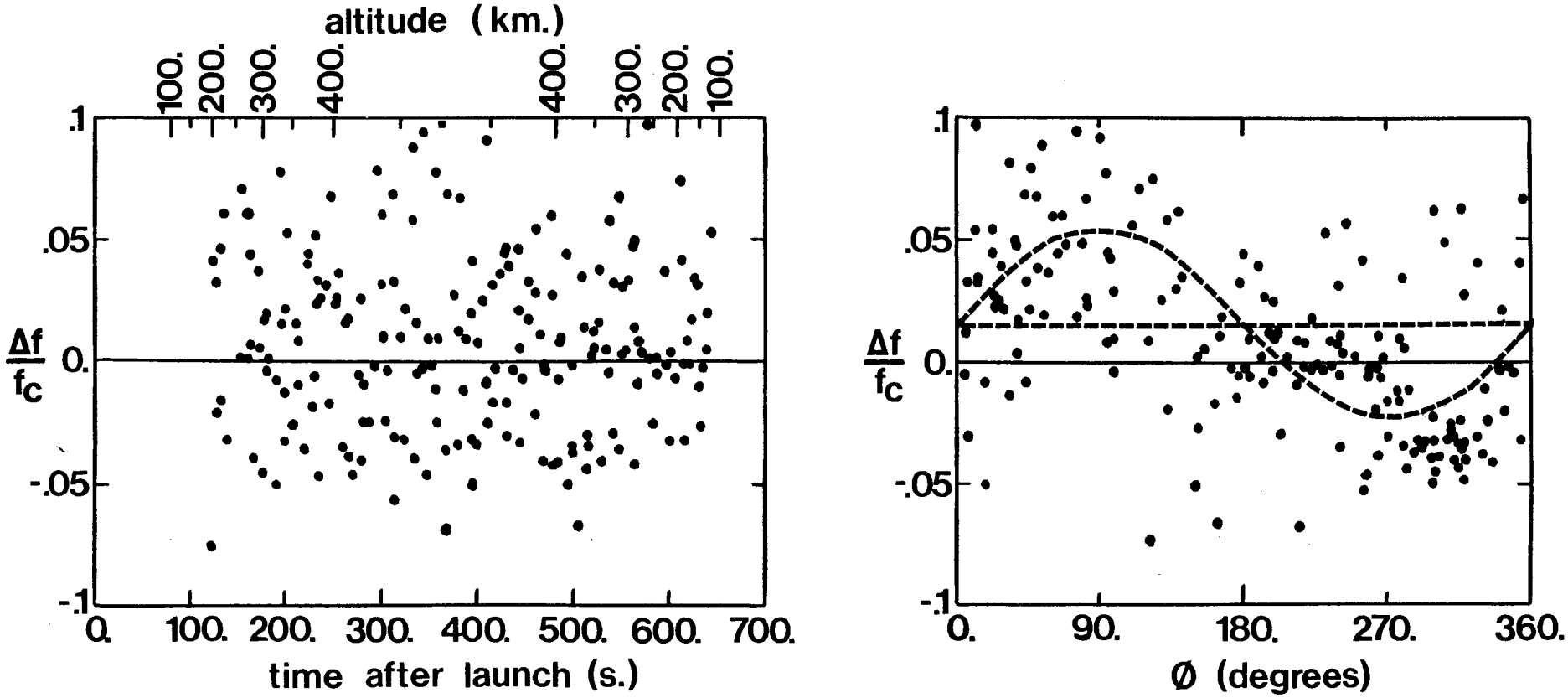
altitude (km.)
100.
200.
300.
400.
400.
300.
200.
100.
.1
.05
0.
-.05
-.1
Δf/fc
0.
100.
200.
300.
400.
500.
600.
700.
time after launch (s.)
(a)
.1
.05
0.
-.05
-.1
Δf/fc
0.
90.
180.
270.
360.
Ø (degrees)
(b)

FIGURE 13.

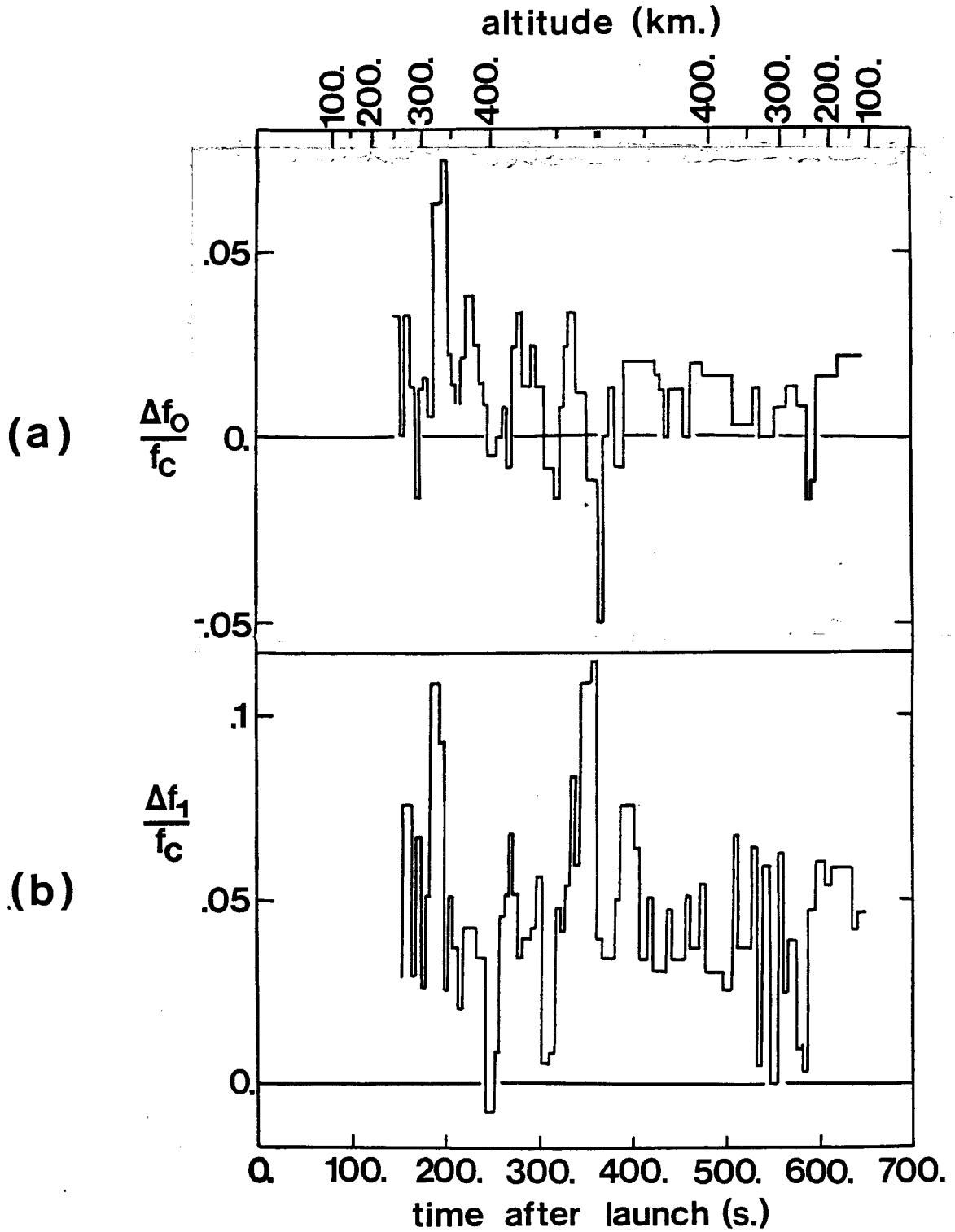
altitude (km.)
100.
200.
300.
400.
400.
300.
200.
100.
(a)
$\frac{\Delta f_o}{f_c}$
.05
0.
-.05
(b)
$\frac{\Delta f_1}{f_c}$
.1
.05
0.
0.
100.
200.
300.
400.
500.
600.
700.
time after launch (s.)

FIGURE 14.

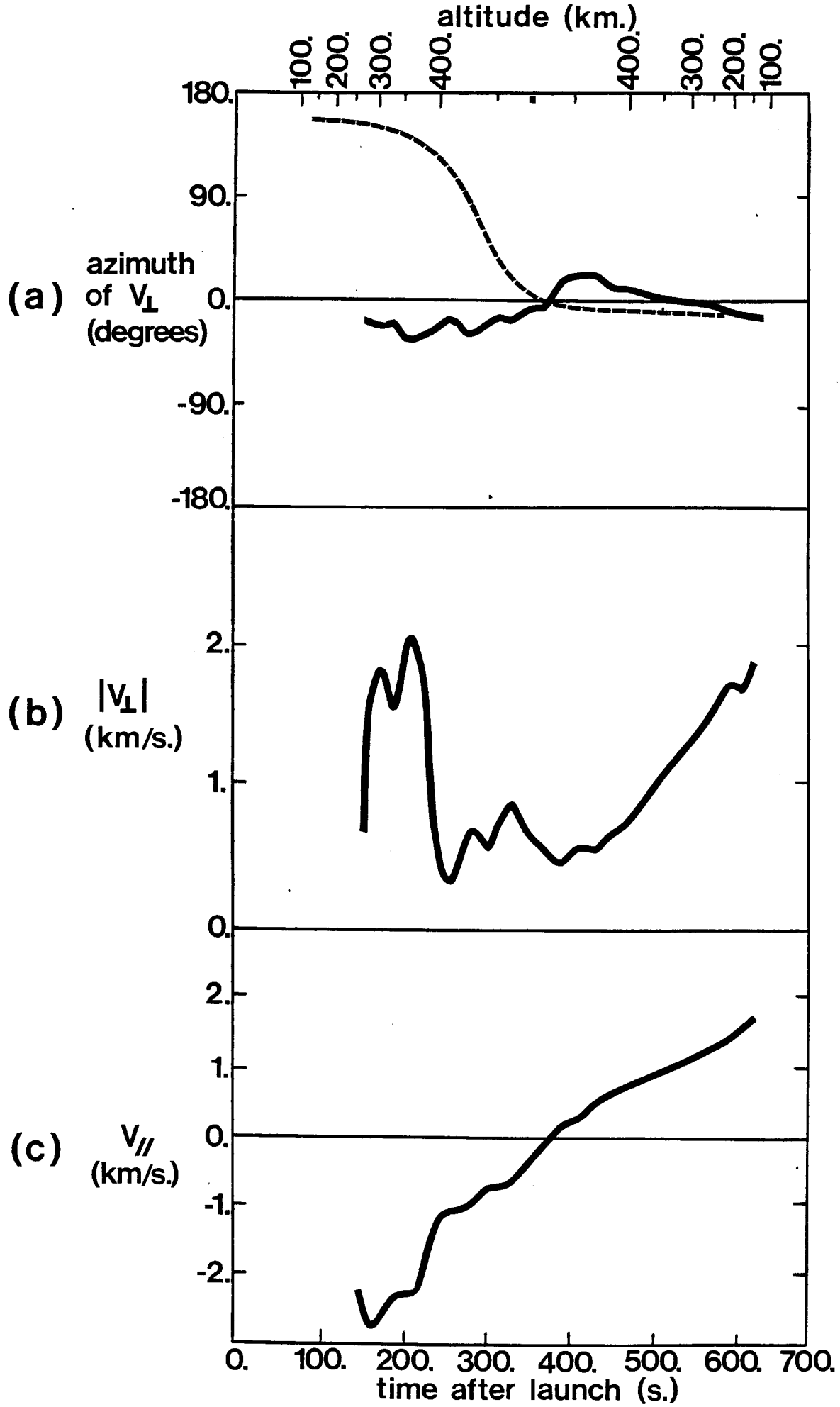
altitude (km.)
100.
200.
300.
400.
400.
300.
200.
100.
180.
90.
azimuth
(a) of $V_\perp$
(degrees)
0.
-90.
-180.
2.
(b) $|V_\perp|$
(km/s.)
1.
0.
2.
1.
(c) $V_{//}$
(km/s.)
0.
-1.
-2.
0. 100. 200. 300. 400. 500. 600. 700.
time after launch (s.)

FIGURE 15.

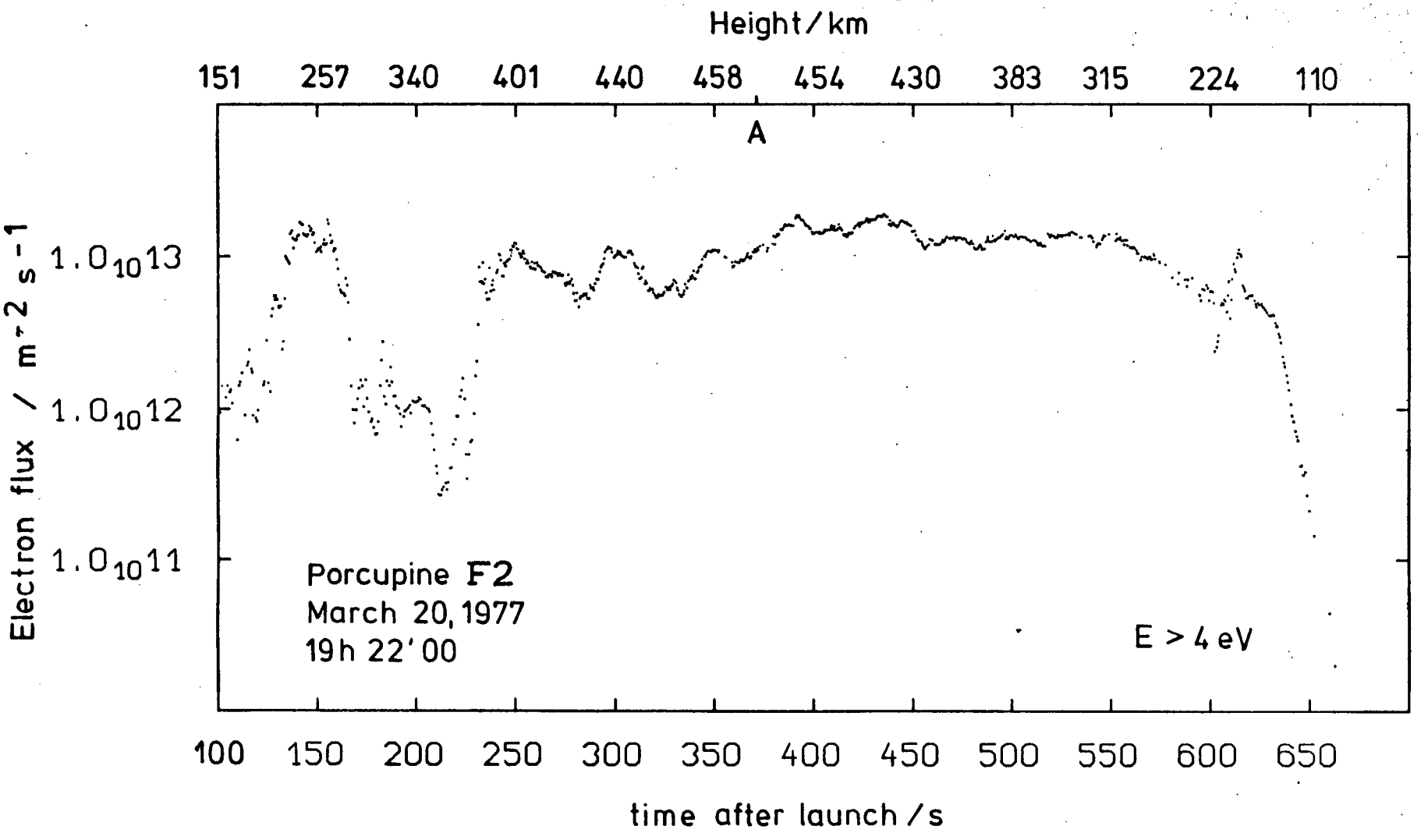
Height / km
151
257
340
401
440
458
454
430
383
315
224
110
A
Electron flux / m⁻² s⁻¹
1.0₁₀13
1.0₁₀12
1.0₁₀11
Porcupine F2
March 20, 1977
19h 22' 00
E > 4 eV
100
150
200
250
300
350
400
450
500
550
600
650
time after launch / s

FIGURE 16.

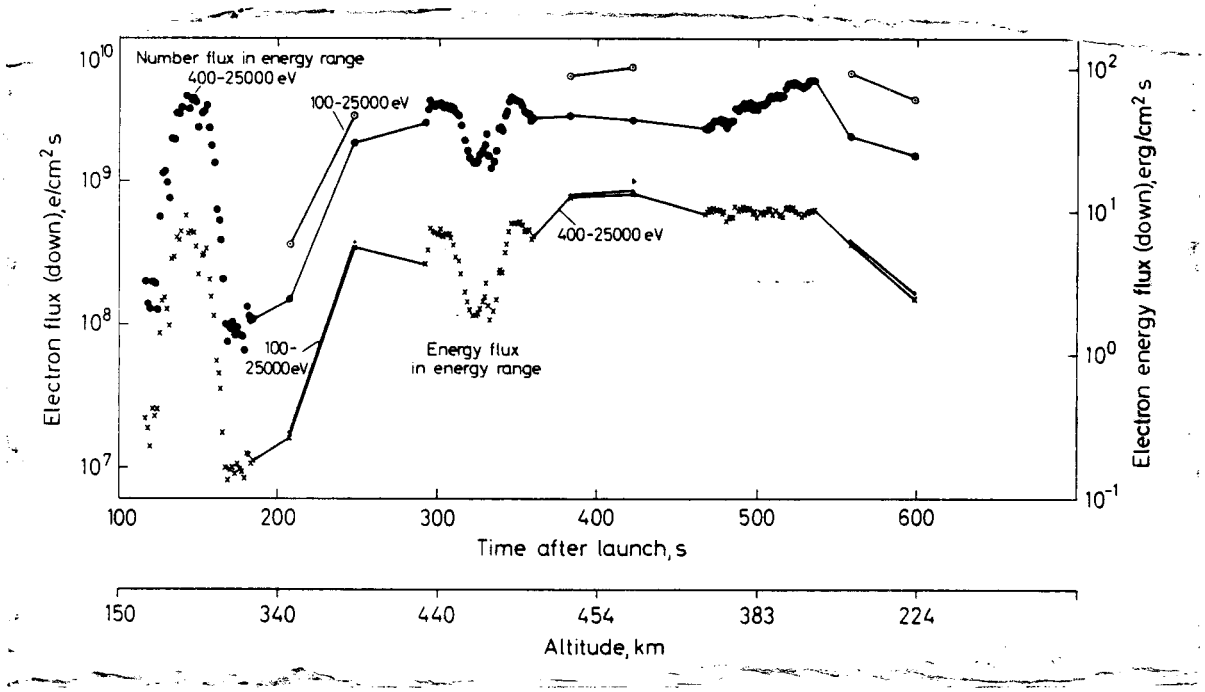
Number flux in energy range
400-25000 eV
100-25000 eV
400-25000 eV
100-
25000eV
Energy flux
in energy range
Electron flux (down), e/cm² s
Electron energy flux (down), erg/cm² s
Time after launch, s
Altitude, km
150
340
440
454
383
224

FIGURE 17.

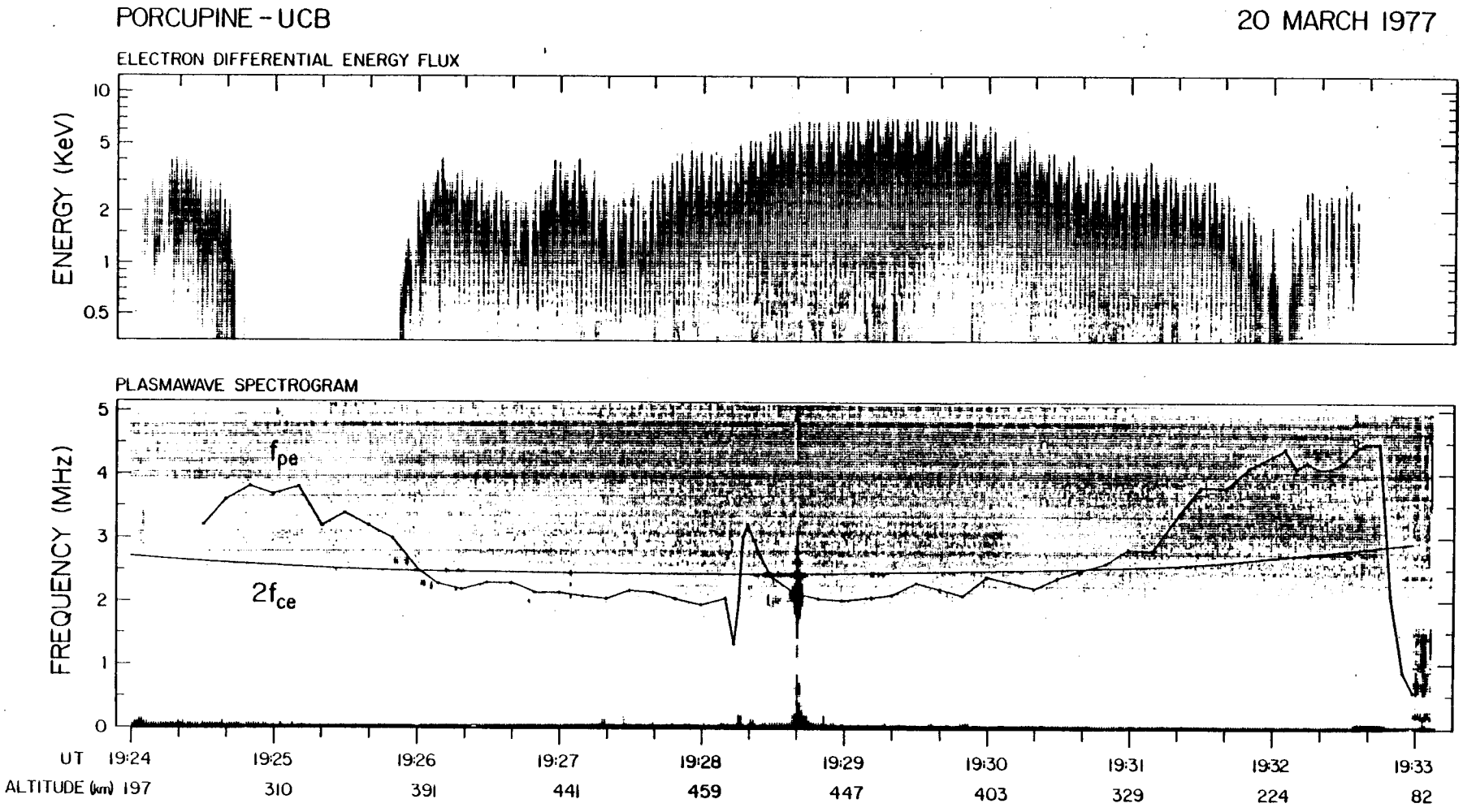
PORCUPINE - UCB
20 MARCH 1977
ELECTRON DIFFERENTIAL ENERGY FLUX
ENERGY (KeV)
10
5
2
1
0.5
PLASMAWAVE SPECTROGRAM
FREQUENCY (MHz)
5
4
3
2
1
0
f_{pe}
$2f_{ce}$
UT 19:24 19:25 19:26 19:27 19:28 19:29 19:30 19:31 19:32 19:33
ALTITUDE (km) 197 310 391 441 459 447 403 329 224 82

FIGURE 18.

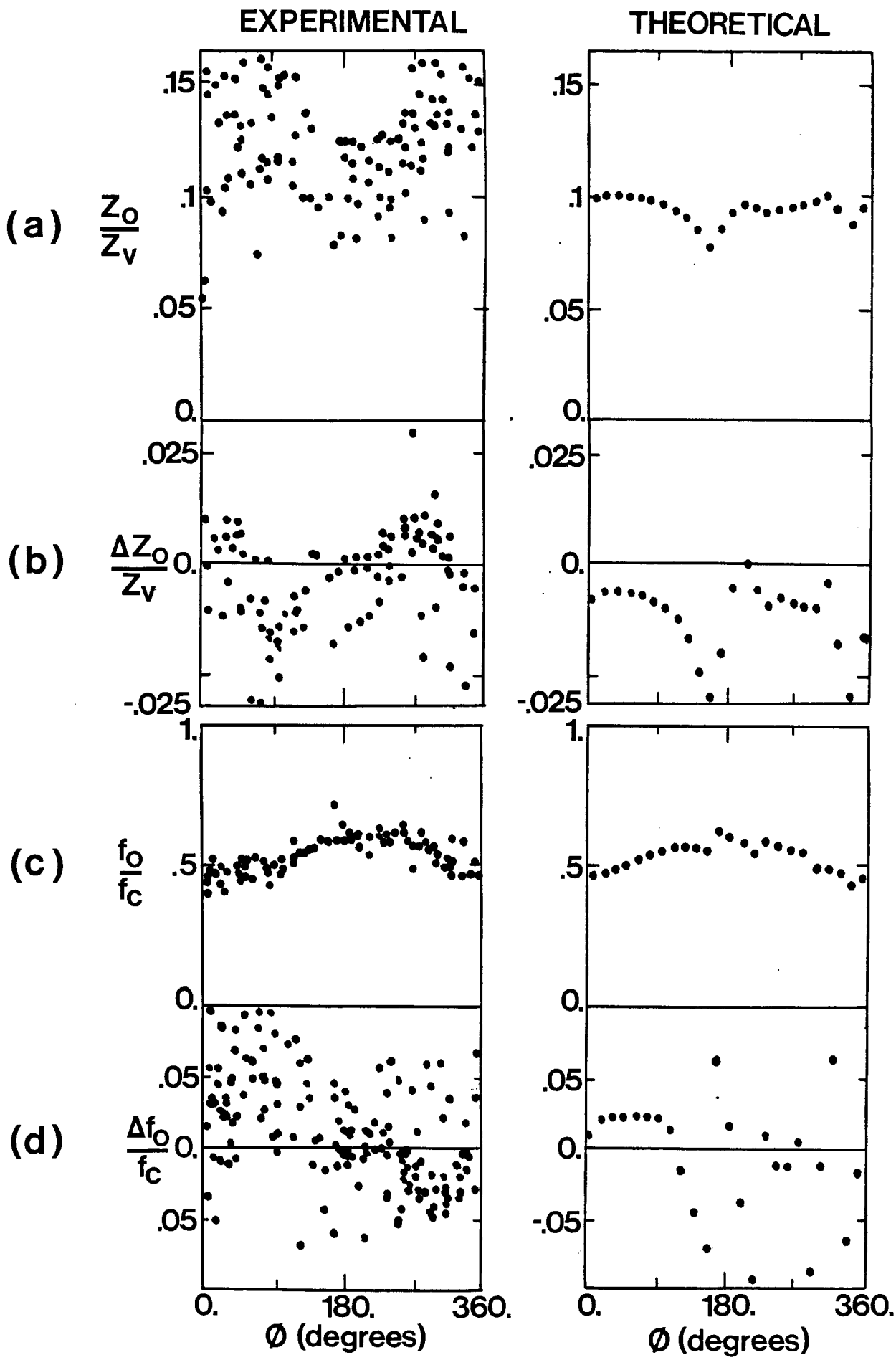
EXPERIMENTAL
THEORETICAL
(a) $\frac{Z_o}{Z_v}$
(b) $\frac{\Delta Z_o}{Z_v}$
(c) $\frac{f_o}{f_c}$
(d) $\frac{\Delta f_o}{f_c}$
.15
.1
.05
0.
.025
-.025
1.
.5
-.05
0.
180.
360.
Ø (degrees)

FIGURE 19.

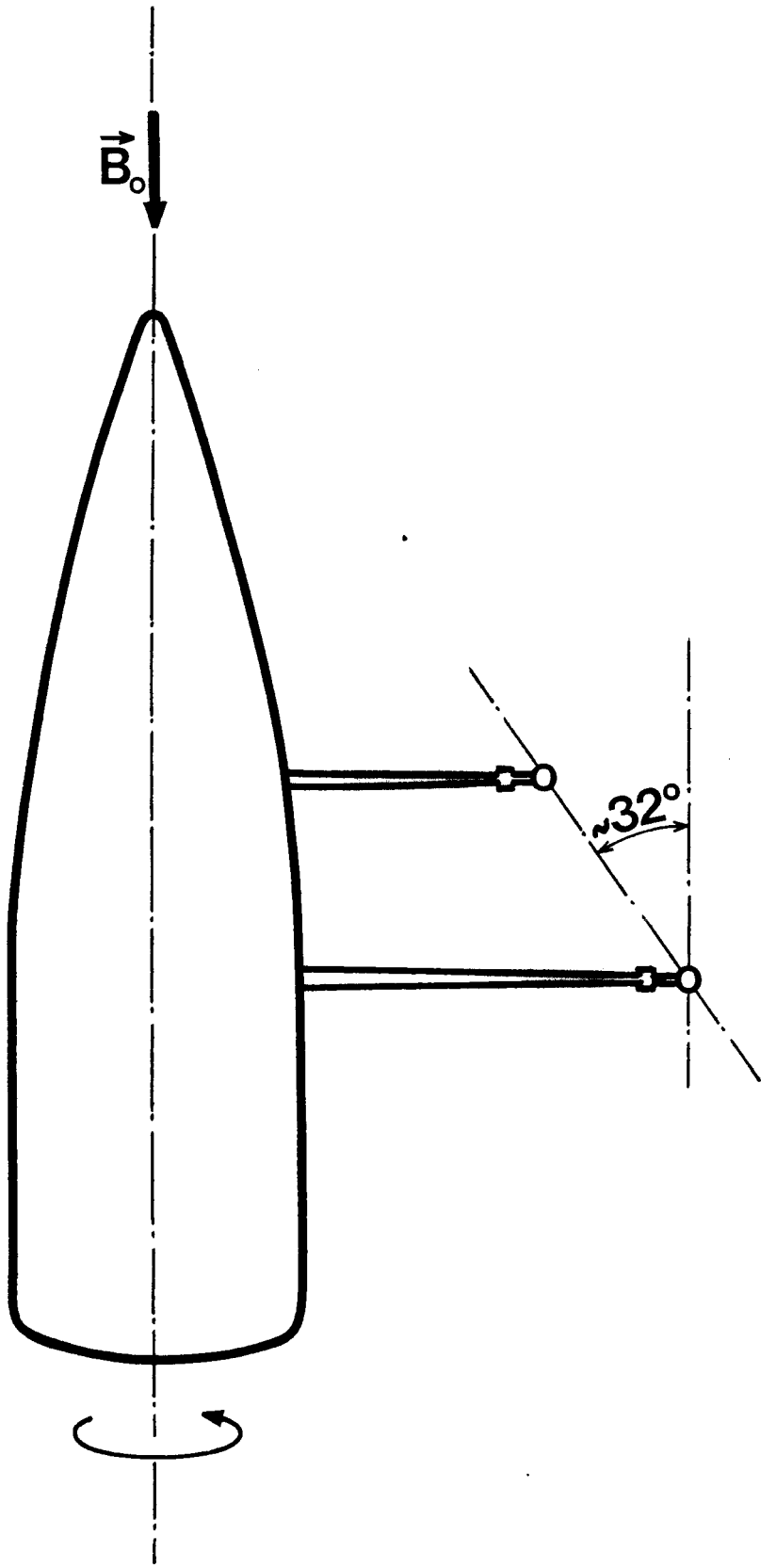

FIGURE 20.

TABLE CAPTIONS

1 Composition of the main payload for the flight F2.

2 Composition of the free-flying sub-payload (Experiment 10) built by the Space Sciences Laboratory of the University of California at Berkeley.

Experiment n°	Parameters measured	Instrument	Institute	Investigators
1A	DC electric field (3-axis)	Double probe	Fraunhofer-Institut für Physikalische Weltraumforschung	R. Grabowski H. Wolf
1B	AC electric field (3-axis)	Double probe	European Space Technology Centre	A. Pedersen
2	Electron density fluctuations	Electrostatic probe	Cornell University	M.C. Kelley
3	Electron energy spectra (0-30 eV)	Retarding-potential analyser	Fraunhofer-Institut für Physikalische Weltraumforschung	K. Spenner W. Ott
4,5	Thermal electrons (see text)	Mutual-impedance probes (see text)	Centre de Recherche en Physique de l'Environnement	L.R.O. Storey J.M. Illiano J. Thiel
6	DC magnetic field (3-axis)	Fluxgate magnetometer	Technische Universität Braunschweig	B. Theile
7	AC magnetic field (1-axis)	Search coil	Max-Planck-Institut für Extraterrestrische Physik	B. Häusler (M.C. Kelley)
8A	Electron energy spectra (0.1-25 keV)	Electrostatic analyser	Max-Planck-Institut für Aeronomie	K. Wilhelm, K.H. Saeger, C. Becker, R. Schmidt W. Engelhardt
8B	Proton energy spectra (1-25 keV)	Electrostatic analyser	Technische Hochschule Graz	W. Riedler A. Dallas
9	Energy spectra Electrons (15-200 keV) Protons (25-2000 keV)	Magnetic spectrometer	Max-Planck-Institut für Aeronomie	W. Stüdemann A. Korth H.P. Winterhoff
10	See Table II	Ejectable sub-payload	University of California Berkeley	F.S. Mozer, K.A. Anderson C.W. Carlson, (M.C. Kelley)
11	DC electric field	Barium ion jets (2 canisters)	Max-Planck Institut für Extraterrestrische Physik	G. Haerendel, A. Valenzuela E. Rieger, H. Föppl
12	Dynamics of Cs plasma beam	Cesium plasma source	USSR Academy of Sciences (1) IKI (2) IZMIRAN	R.Z. Sagdeev (1), I.A. Zhulin (2), V.A. Dukukine (2), J.J. Ruzhin (2) (G. Haerendel)

TABLE 1

Parameters measured	Range	Techniques
Electron energy spectra	1 - 500 eV at 3 pitch angles	Channeltrons in retarding potential analysers
Electron energy spectra	0.5 - 40 keV at 1 pitch angle	Channeltrons in electrostatic analysers
Positive ion energy spectra	0.5 - 40 keV at 1 pitch angle	Channeltrons in electrostatic analysers
H^+, H_e^+, H_e^{++}, CNO^+ energy/(unit charge)	0.5 - 40 keV/charge	Solid-state detectors in electrostatic analysers
DC electric field	1 - 100 mV/m	Three orthogonal double-probe sensors
AC electric field	0 - 5 MHz	
Thermal electron density	10^3 - 10^6 cm^{-3}	Modulated electrostatic probes
Thermal electron temperature	500 - 4000 K	
Electron density fluctuations	0 - 1000 Hz $\Delta n/n > 0.01$	
Electron temperature fluctuations	0 - 100 Hz $\Delta T/T > 0.01$	
Magnetic field variations	$\Delta B > 30\ \gamma$	Fluxgate magnetometer

TABLE 2